UNIVERSITY OF CALGARY

Near-term quantum repeaters

by

Yufeng Wu

A THESIS

SUBMITTED TO THE FACULTY OF GRADUATE STUDIES

IN PARTIAL FULFILLMENT OF THE REQUIREMENTS FOR THE

DEGREE OF MASTER OF SCIENCE

GRADUATE PROGRAM IN PHYSICS AND ASTRONOMY

CALGARY, ALBERTA

AUGUST, 2020

Abstract

Future quantum networks will enable fascinating applications such as secure communication, quantum-enhanced distributed sensing, distributed quantum computing, and accurate global time-keeping. Center to these applications is quantum entanglement distribution, whose effective distance is limited by photon loss. Quantum repeaters were proposed to extend the effective distance, but their demonstration has not been reported yet.

In this thesis, we study quantum repeaters with both single-emitter based and ensemble-based quantum memories. In particular, we study the feasibility of meaningful proof-of-principle demonstrations of several quantum repeater protocols (with two-links) with photon (single-photon and photon-pair) sources and atomic-ensemble based quantum memories. We take into account non-unit memory efficiencies that decay exponentially with time, which is more realistic and accurate compared to previous treatments. We discuss implementations based on quantum dots, parametric down-conversion, rare-earth-ion doped crystals, and Rydberg atoms. Our results provide guidance for the near-term implementation of long-distance quantum repeater demonstrations, suggesting that such demonstrations are within reach of current technology.

Acknowledgements

First of all, I wish to express my sincere appreciation to my supervisor, Prof. Christoph Simon for his supportive, patient, and insightful guidance. Christoph is an easy-going supervisor, so in the two-year life as a master student, I literally had no pressure from the academic side, which was unexpected. At the same time, Christoph cares about students' research progress and makes sure everyone is on the right track. He always generously provide his insightful suggestions and useful materials whenever his student is asking. Christoph also cares about students' future. After knowing my plans for Ph.D. applications, he was very supportive and told me all his connections unreservedly, and undoubtedly this was of vital importance in my application process.

I would like to thank all my friends. I want to send my special regards to Jiawei, who helped me rent the house and settle down when I came to Calgary and introduced me to many friends. On the academic side, he is also a good collaborator and I have learned a lot from him. I also thank Sumit, Faezeh, Sourabh, Parisa, Farid, Stephen, Ken, and Jordan who helped me in both research and life. I enjoy the time chatting, discussing novel ideas and hard problems, and doing light exercises in the office.

I would also like to thank Prof. Barry Sanders, David Hobill, and David Feder who have taught me in different courses. They are responsible and knowledgeable, and I have learned a lot from them and the classes.

I would like to pay my special regards to my parents for providing me with unfailing support and continuous encouragement throughout my years of study and through the process of researching and writing this thesis. This accomplishment would not have been possible without them. Thank you!

List of papers published, submitted, or to be submitted

Wu, Yufeng, Jianlong Liu, and Christoph Simon. "Near-term performance of quantum repeaters with imperfect ensemble-based quantum memories." **(Editor's suggestion)** Physical Review A 101, no. 4 (2020): 042301.

Wein, Stephen C., Jia-Wei Ji, **Yu-Feng Wu**, Faezeh Kimiaee Asadi, Roohollah Ghobadi, and Christoph Simon. "Analyzing photon-counting based entanglement generation between solid-state spin qubits by unraveling the master equation." arXiv preprint arXiv:2004.04786 (2020).

Jia-Wei Ji, **Yu-Feng Wu**, Stephen C. Wein, Faezeh Kimiaee Asadi, Roohollah Ghobadi, and Christoph Simon. "Proposal for a room-temperature quantum network with diamonds and optomechanics at telecommunication wavelengths" In preparation.

Table of Contents

List of Tables

List of Figures and Illustrations

List of Symbols, Abbreviations and Nomenclature

Symbol	Definition
U of C	University of Calgary
DLCZ	Duan, Lukin, Cirac, and Zoller
PDF	Probability density function
SPS	Single photon source
dPPS	Deterministic photon-pair source
ndPPS	Non-deterministic photon-pair source
BSM	Bell-state measurement
EDT	Entanglement distribution time
QDs	Quantum dots
RAs	Rydberg atoms
REIs	Rare-earth ions
(S)PDC	(Spontaneous) parametric down-conversion
FWM	Four-wave mixing
AFC	Atomic frequency comb
The “1 + 1” scheme	SPS with single-photon BSM scheme
The “2 + 2” scheme	dPPS with two-photon BSM scheme
The “$\tilde{2}$ + 1” scheme	ndPPS with single-photon BSM scheme
The “$\tilde{2}$ + 2” scheme	ndPPS with two-photon BSM scheme

Chapter 1

Introduction

Quantum mechanics enable information processing using quantum mechanical systems that could offer advantages over classical counterparts. This type of information processing is called "quantum information processing". Classical information processing is based on classical bits that can be either 0 or 1, while quantum information processing is based on quantum bits (qubits) that can exist in a superposition of both 0 and 1.

Coherence and entanglement are the most striking features of a quantum system. For a single qubit, the quantum state is characterized by the superposition

$$\alpha\,|0\rangle + \beta\,|1\rangle\,,$$

where $|0\rangle$ and $|1\rangle$ are two possible states, and $|\alpha|^2+|\beta|^2= 1$. Taking the example of the famous Schrödinger's cat experiment, the cat is in a superposition state where "dead" and "alive" are the two possible states. Let us assume that the macroscopic superposition is possible here. Once we open up the box, i.e., perform a measurement, we can find the state of the cat collapse to one of the possible states, either dead or alive. This is fundamentally different from a classical object. To illustrate, let us imagine a precise machine that could toss a coin such that the probability of heads up and tails up are $|\alpha|^2$ and $|\beta|^2$, respectively. The machine tosses a coin in a closed box that no one could get any information from it without opening the box. The state of the coin is either heads up or tails up, but it is not a superposition state because there is no coherence. In the case of Schrödinger's cat, α and β are complex amplitudes and thus the state has encoded phase information. Therefore, to determine the original quantum state, the measurement in the basis of $|0\rangle$ and $|1\rangle$ is not enough, although it can give the information about the probabilities, i.e., $|\alpha|^2$ and $|\beta|^2$. To know the phase information, one has to measure the state in a different basis. In contrast, the state for tossing a coin can be deduced by only repeated measurement of the statistics of "0"

(heads) and "1" (tails).

The entanglement was described as "spooky interaction at a distance" by Albert Einstein, and it is indeed a mystery. For a pair or group of particles, the quantum state can have an interesting form, such as

$$\alpha\,|00\rangle + \beta\,|11\rangle\,,$$

where $|00\rangle$ and $|11\rangle$ are bipartite quantum states, and $|\alpha|, |\beta| > 0$. Say Alice has prepared such a state and send one of the qubits to Bob. If Alice measures the state of her qubit, she can immediately determine the state of Bob's qubit. However, there is no information transmitted to Bob, unless Alice communicated with Bob through a classical communication channel, and thus it does not violate Einstein's theory of relativity that states transmission of the information at faster-than-light speeds is impossible [1].

Quantum computation and quantum communication are two important subfields of quantum information processing [1]. In 1982, Richard Feynman proposed the idea that a computer made of quantum systems might simulate quantum systems more efficiently than state-of-the-art classical computers [2]. Besides, after Shor's [3] and Grover's [4] algorithms were discovered, much interest was attracted by quantum algorithms that could provide spectacular speedup. A recent experiment has demonstrated a quantum device that can solve a problem faster than classical computers [5]. However, the quantum advantage in solving a meaningful problem has not been reported. On the other hand, the foundation of quantum communication theory starts with the work of Stephen Wiesner and Gilles Brassard on quantum conjugate coding [6]. In 1984, Gilles Brassard and Charles H. Bennett came up with the first practical secure communication protocol: BB84 protocol [7]. The security of quantum communication is proved in various conditions [8–10]. To implement quantum communication over a long distance, the ideal information carriers are photons that can be transmitted via either optical fiber or free space. One impressive demonstration of free-space quantum key distribution is between the ground station and the low-Earth-orbit satellite with a distance up to 1200 km [11, 12]. For fiber-based quantum key distribution, the longest distance that

has been achieved is 421 km [13]. To extend the distance, one has to overcome the loss of photons that has exponential scaling with distance through the optical fiber. As no-cloning theorem makes the amplification of the unknown quantum state impossible [14], quantum repeaters are proposed to extend the secure communication distance [15].

1.1 Quantum repeaters

The basic idea of quantum repeaters is to divide the transmission channel into many segments, with the length of each segment that is comparable to the channel attenuation length. First, entanglement is generated and purified for each segment; the purified entanglement is then extended to a greater length by connecting two adjacent segments through entanglement swapping. After this swapping, the overall entanglement is decreased and has to be purified again [15]. The rounds of entanglement swapping and purification can be continued until nearly perfect entangled states are created between two distant sites [16]. Therefore, by dividing a sufficient number of segments, a higher rate compared to direct transmission is possible in the long distance.

1.2 Quantum networks: implementations and challenges

Quantum networks are networks that can distribute quantum states and quantum entanglement (between any two points on the earth), which promises applications such as secure communication, quantum-enhanced distributed sensing, and distributed quantum computing [17–19]. Several major applications have already been demonstrated, including practical quantum key distribution [11, 12, 20, 21], small qubit-number quantum links [22, 23], and etc. These demonstrations mark that we are now at an exciting moment in time.

Quantum key distribution has been tested and implemented over metropolitan distances [24–26], and much longer quantum repeater links are investigated by many countries. The current focus of quantum repeater is mainly aiming for entanglement distribution with more than 500 km, because direct transmission is a better choice for a shorter distance. For a distance of a few thousand

kilometers, the use of low-Earth-orbit satellite links may be the optimum solution. Therefore, the fiber-based quantum repeaters are preferred in the distance range of 500 - 2000 km [18]. However, no such quantum repeaters have been demonstrated and one should recognize we are still at the initial stage towards global quantum networks [19]. The main challenge is the imperfect quantum devices in the near-term. To be specific, they are photon sources, quantum memories, and photon detectors.

Photon sources. To minimize the photon loss in the optical fiber, the wavelength of the emitted photon should match the telecom wavelength that is around 1550 nm. Besides, an ideal photon source should also have unity indistinguishability and zero multi-photon(pair) emission ($g^{(2)}(0)$). For deterministic photon sources, the "on-demand" photon emission is necessary; for non-deterministic photon sources such as those based on parametric downconversion (PDC) and four-wave mixing (FWM), the multi-photon pair emission is unavoidable, and one has to sacrifice the probability of generating a single pair to decrease $g^{(2)}(0)$. It is important to note that the boundary between deterministic photon source and probabilistic photon source is not clear. An example of this is seen when a source classified as deterministic has a loss in the extraction of the photon from the region where it is generated. As that emission (or extraction) loss increases, a theoretically deterministic source becomes more probabilistic in operation. In recent experiments, near-perfect performance has been shown in each of these criteria, while no one has demonstrated them all in a single source. The repeater performance can be improved in a multiplexing scheme that could require the photon sources emitting multiple photons (or pairs) in time, space, or frequency.

Quantum memories. Quantum memories are necessary components of quantum repeater links to keep the quantum state before entanglement swapping and extend to a longer distance. A quantum memory should have high efficiency, which means it can store and retrieve a single photon with very high probability. The memory lifetime is also of great importance. During the entanglement swapping process, the repeater link which establishes the entanglement earlier should wait for the success of the other link, during which process the memory decays. This will degrade the

state fidelity in the single emitter based memory, or the memory efficiency in an ensemble-based memory [27]. An ideal quantum memory should also have high bandwidth and appropriate wavelength that could match the photon sources. Furthermore, in the multiplexing repeater schemes, quantum memories should have the capacity to store multiple photons and dimensionality (time, space, or frequency).

Photon detectors. Photon detectors are used in the Bell-state measurement process, where a beam-splitter erases the which-path information and the photon detector detects the photon to create entanglement. An ideal photon detector should satisfy two important criteria: the probability that a photon incident upon the detector is successfully detected is 100% (unity detection efficiency) and the rate of detector output pulses in the absence of any incident photons is zero (zero dark-count rate). The imperfect photon detection will reduce the fidelity of the entangled state and the success probability of the entanglement generation/swapping process. For quantum repeater protocols that rely on photon counting measurements, the ability to distinguish the number of photons in an incident pulse (photon-number resolution) could improve the state fidelity [28].

Besides the imperfect quantum devices, other challenges such as the integration of different components, making many identical photon sources and quantum memories, frequency conversion (or quantum transduction), and the ability to perform entanglement purification and error-correction is non-negligible. Although it is hard to predict what exactly the required components for the first generation of quantum networks will be, it is likely that we will see its birth within the next few years.

1.3 Our focus in this thesis

In this thesis, we will focus on quantum repeaters in the near-term, and specifically, we analyze the performance of a two-link quantum repeater with ensemble-based memories. Chapter 2 gives a general introduction to quantum repeaters, including the basic procedures of using quantum repeaters, criteria of a quantum repeater, and the difference between single-emitter based quantum

repeaters and ensemble-based quantum repeaters. Chapters 3 and 4 then review quantum repeater protocols with single emitter and ensemble-based memories, respectively, where the performance of the protocols is analyzed in detail (without considering the memory decay). In Chapter 5, we take memory decay into consideration and give an estimation of performance for a two-link quantum repeater with ensemble-based quantum memories. This work has been published in Physical Review A [29].

Chapter 2

Quantum repeaters

2.1 Basics of quantum repeaters

The key idea of quantum repeaters is that a distance L can be divided into multiple segments where entanglement can be generated and stored independently in these segments and then extended via entanglement swapping. Many quantum repeater protocols have been proposed and being realized in a toy model (with only one link) [30]. In this section, we give a brief introduction to a general quantum repeater.

2.1.1 An elementary link

An elementary link is the basic unit of a quantum repeater, where each elementary link contains two remote nodes with one in each end. Each node contains at least one or two quantum memories that store and retrieve the quantum information. Besides quantum memories, photon sources may be necessary to create the initial memory excitation, especially for ensemble-based quantum memories. In the middle of the two nodes is a Bell-state measurement platform that is essential in the entanglement generation step.

2.1.2 Entanglement generation

In the entanglement generation process, two remote memories in an elementary node are entangled. This is usually done by first creating memory-photon entanglement, and then the photons are sent to a central beam-splitter. After the beam-splitter erases the which-path information, the two memories are entangled in the corresponding encoding space.

As the photon loss and detection error are inevitable, the entanglement generation process is probabilistic. As a result, the entanglement generation attempt that does not give the desired

detector click will be aborted and the whole process should start over again.

2.1.3 Entanglement swapping

Once the entanglement is generated in all the elementary links, the entanglement should be swapped between the neighboring links. To do so, a two-qubit gate should be applied to the two memories followed by corresponding measurements. Depending on the different entanglement swapping schemes, the process can be deterministic or probabilistic. For probabilistic entanglement swapping, an undesired measurement result will destroy the whole state associated with the two memories, and thus the process should start over from the entanglement generation process. A nested repeater structure may require multiple rounds of entanglement swapping process. After each round, the entanglement is distributed over a double distance. For probabilistic entanglement swapping, the success probability will limit the repeater rates since each failed attempt will make everything start over again. On the other hand, if the entanglement swapping process is deterministic, the start-over is not necessary and thus the repeater rate can be significantly higher.

2.1.4 Entanglement purification

The original quantum repeater proposed by Briegel, Dür, Cirac and Zoller (BDCZ scheme) also contains entanglement purification steps that mitigate the effect of decoherence [15]. The implementation of entanglement purification requires extra links in each nesting level, leading to a higher fidelity but lower rates. Due to the imperfect quantum devices' performance in the near-term, the impact on rates to increase the fidelity a fair amount is forbidding, and thus entanglement purification is not within consideration in this thesis.

2.2 Performance criteria

Repeater rates and fidelity of the final entangled state are the two most critical figure of merit. Direct transmission is limited to a distance of several hundred kilometers, so for the repeater rates,

the ultimate goal is to beat the direct transmission and make quantum key distribution and other applications possible for longer distances. The repeater rates are limited by the various imperfections of the quantum devices including detector efficiency, efficiency and lifetime of quantum memories, and efficiency of photon sources.

On the other hand, the imperfect entanglement swapping operation, memory decay/decoherence, non-perfect photon sources, and dark counts may degrade the fidelity. Entanglement purification is essential to distill highly entangled states from less entangled ones, while it requires at least 50% original fidelity [31]. However, in the near-term quantum network implementations, the fidelity is required to be higher than 90% to minimize the use of quantum purification.

2.3 Single-emitter based quantum repeaters

Single-emitter based quantum repeaters use single-emitter systems as quantum memories. These quantum emitters have properties resembling those of atoms and ions and can realize spin-photon interference in a scalable and compact manner [32]. These quantum emitters are usually these embedded in material platforms that enable the stable spin and optical properties such as silicon (various radiation damage centers) and carbon (SiV centers, NV centers), as well as rare-earth-ion-doped crystals, trapped ions and atoms, and semiconductor quantum dots. Solid-state single-emitter is also attractive for the accessibility of nuclear spins, making it possible that the quantum states can be stored both in electronic spins and nuclear spins. Due to the high fidelity quantum gate between electronic spins and nuclear spins, the quantum repeaters schemes have more flexible entanglement swapping schemes.

It is important to note that single-emitter based quantum memories are subject to the dephasing process that comes from the interaction of the spin qubit with a nuclear spin bath [33] or lattice phonons [34]. In the context of quantum repeaters, such spin decoherence will decrease the fidelity of the final entangled state. Thus, in a realistic quantum repeater, quantum error-correction [35] or entanglement purification [31] are necessary for long-distance entanglement distribution.

2.4 Ensemble based quantum repeaters

Quantum repeaters with ensemble-based memories are of particular interest in quantum repeater applications since the first realistic implementation proposal by Duan, Lukin, Cirac, and Zoller (DLCZ scheme) [36]. Quantum states are stored as collective excitation, i.e., states that are a coherent superposition of all possible atoms' excited state. Such a collective excitation state is of great interest for practical applications since the state can be efficiently readout by converting them into single photons that propagate in a well-defined direction [36]. Ensemble-based quantum memories are also subject to decoherence, in contrast to the scenario of single-emitter quantum memories, which results in a reduction of efficiency rather than fidelity [27].

Some ensemble-based quantum memories such as rare-earth-ion doped crystals are also attractive for broad inhomogeneous linewidths. This enables multiple-photon and multiple-mode storage capacity using schemes such as atomic frequency comb (AFC), which will greatly enhance the repeater rates [37].

Chapter 3

Single-emitter based quantum repeater protocols

3.1 Entanglement generation protocols

There have been many entanglement generation schemes for single-emitter based quantum repeaters [38–47]. In this section, we only focus on a three level system that has an excited state $|e\rangle$ and two ground states $|\uparrow\rangle$ and $|\downarrow\rangle$, where transition $|\downarrow\rangle$ to $|e\rangle$ is forbidden.

3.1.1 Single-photon detection protocol

One simple method of generating entanglement between two remote emitters begins with each emitter in state

$$\sin(\phi)\,|\uparrow\rangle + \cos(\phi)\,|\downarrow\rangle\,, \tag{3.1}$$

where $\sin(\phi) \ll 1$ to reduce the two-photon emission event. The π pulse that excites state $|\uparrow\rangle$ to $|e\rangle$ is applied to both emitters, with resultant state of the two system

$$(\sin(\phi)\,|e\rangle + \cos(\phi)\,|\downarrow\rangle) \otimes (\sin(\phi)\,|e\rangle + \cos(\phi)\,|\downarrow\rangle). \tag{3.2}$$

After sufficient time to eliminate all the excitation, the state is now

$$\sin^2(\phi)\,|\uparrow\uparrow\rangle\,|11\rangle + \sin(\phi)\cos(\phi)(|\uparrow\downarrow\rangle\,|10\rangle + |\downarrow\uparrow\rangle\,|01\rangle) + \cos^2(\phi)\,|\downarrow\downarrow\rangle\,|00\rangle\,, \tag{3.3}$$

with photon mode $|1\rangle$ and $|0\rangle$. The photon emitted is sent to a central beam-splitter that erases the which-path information, after which the photon is measured by a detector. With a single detector click, the state becomes

$$\frac{\sin(\phi)}{\sqrt{1+\cos^2(\phi)}}\,|\uparrow\uparrow\rangle + \frac{\cos(\phi)}{\sqrt{1+\cos^2(\phi)}}(|\uparrow\downarrow\rangle \pm |\downarrow\uparrow\rangle), \tag{3.4}$$

with probability $\sin^2(\phi)(1+\cos^2(\phi))$, where the $\pm$ sign is determined by which detector clicked. The "unwanted state" $|\uparrow\uparrow\rangle$ is created because we assume the detector cannot resolve photon number. The fidelity is thus $2\cos^2(\phi)/(1+\cos^2(\phi))$.

System limitation. To include realistic imperfections, here we use conditional evolution method, where the time dynamics of the entanglement generation process by unraveling a Markovian master equation into a set of propagation superoperators conditioned on the cumulative detector photocount [28]. Considering optical decay rate γ, optical dephasing rate $\gamma^\star$, and spin dephasing rate γ_s, photon detection efficiency η, and the duration of the detection window t_d, the density matrix in the limit $\gamma t_d \gg 1$ is

$$\rho = p_{\uparrow\uparrow}|\uparrow\uparrow\rangle\langle\uparrow\uparrow| + \frac{1}{2}p_0(|\uparrow\downarrow\rangle\langle\uparrow\downarrow| + |\downarrow\uparrow\rangle\langle\downarrow\uparrow|) + p_c(|\uparrow\downarrow\rangle\langle\downarrow\uparrow| + |\downarrow\uparrow\rangle\langle\uparrow\downarrow|) \tag{3.5}$$

where $p_{\uparrow\uparrow} = [\eta\sin^4(\phi)(\gamma(2-\eta)+(4-3\eta)(\gamma^\star+\gamma_s))]/2(\gamma+2(\gamma^\star+\gamma_s))$, $p_0 = \eta\sin^2(2\phi)/4$ is the success probability, and $p_c = \gamma\eta\sin^2(2\phi)e^{-2t_d\gamma_s}/8(2\gamma^\star+\gamma-2\gamma_s)$. The total success probability is thus

$$p = 2(p_{\uparrow\uparrow}+p_0) = \frac{\eta\sin^4(\phi)(\gamma(2-\eta)+(4-3\eta)(\gamma^\star+\gamma_s))}{\gamma+2(\gamma^\star+\gamma_s)} + \frac{\eta\sin^2(2\phi)}{2}, \tag{3.6}$$

where the prefactor "2" represents two possible detector click, and the fidelity is

$$\begin{aligned} F &= \frac{1}{2} + \frac{p_c}{2(p_{\uparrow\uparrow}+p_0)} \\ &= \frac{1}{2}(1 + \frac{\gamma\eta\sin^2(2\phi)e^{-2t_d\gamma_s}}{8(2\gamma^\star+\gamma-2\gamma_s)} \frac{4(\gamma+2(\gamma^\star+\gamma_s))\csc^2(\phi)}{\eta(\gamma(\eta\cos(2\phi)-\eta+4)+(\gamma^\star+\gamma_s)(3\eta\cos(2\phi)-3\eta+8))}). \end{aligned} \tag{3.7}$$

In the limit $\phi \to 0$, the fidelity has an upper bound

$$F_{\phi\to 0} = \frac{1}{2}(1 + \frac{\gamma\left(e^{-2t_d\gamma_s} - e^{-t_d(2\gamma^\star+\gamma)}\right)}{(2\gamma^\star+\gamma-2\gamma_s)(1-e^{-t_d\gamma})}). \tag{3.8}$$

Thus, the fidelity decays exponentially with spin dephasing rate and is limited by the indistinguishability $\gamma/(\gamma+2\gamma^\star)$.

3.1.2 Two-photon detection protocol

Another protocol proposed by Barrett and Kok (B-K scheme) [41] uses two-photon detection. The scheme starts with both emitters in state

$$\frac{1}{\sqrt{2}}(|\uparrow\rangle + |\downarrow\rangle). \tag{3.9}$$

Then π pulses are applied to both emitter to excite state $|\uparrow\rangle$ to state $|e\rangle$, and the resultant state is

$$\frac{1}{2}(|e\rangle + |\downarrow\rangle) \otimes (|e\rangle + |\downarrow\rangle). \tag{3.10}$$

After sufficient time to eliminate all the excitation, the state is now

$$\frac{1}{2}(|\uparrow\uparrow\rangle |11\rangle + |\uparrow\downarrow\rangle |10\rangle + |\downarrow\uparrow\rangle |01\rangle + |\downarrow\downarrow\rangle |00\rangle), \tag{3.11}$$

where $|0\rangle$ and $|1\rangle$ are photon modes. The photon is sent to a central beam-splitter, with a successful click, the state becomes

$$\beta(\eta) |\uparrow\uparrow\rangle + \alpha(\eta)(|\uparrow\downarrow\rangle \pm |\downarrow\uparrow\rangle), \tag{3.12}$$

where α and β depend on the photon loss η. Here $|\uparrow\uparrow\rangle$ remains because the single-photon Bell-state measurement cannot distinguish it and $|\uparrow\downarrow\rangle \pm |\downarrow\uparrow\rangle$. To eliminate the first term, a second detection is needed. A π pulse is applied between $|\uparrow\rangle$ $|\downarrow\rangle$, followed by another π pulse that excite state $|\uparrow\rangle$ to $|e\rangle$. The state is now

$$\beta(\eta) |\downarrow\downarrow\rangle + \alpha(\eta)(|\downarrow e\rangle \pm |e\downarrow\rangle). \tag{3.13}$$

The first term has no contribution to the second detection, and with a successful click it will be eliminated, resulting in the state

$$\frac{1}{\sqrt{2}}(|\downarrow\uparrow\rangle \pm |\uparrow\downarrow\rangle), \tag{3.14}$$

where the $\pm$ depends on the detectors that click in the two rounds. The success probability is $1/2$ (as it only postselects the state $|\downarrow\uparrow\rangle$ and $|\uparrow\downarrow\rangle$ in Eq. 3.11) without photon loss, and the fidelity is 1.

System limitation. Under realistic imperfections, the final density matrix in the limit $\gamma t_d \gg 1$ is

$$\rho = \frac{1}{2} p_0 (|\uparrow\downarrow\rangle \langle\uparrow\downarrow| + |\downarrow\uparrow\rangle \langle\downarrow\uparrow|) + p_c (|\uparrow\downarrow\rangle \langle\downarrow\uparrow| + |\downarrow\uparrow\rangle \langle\uparrow\downarrow|), \tag{3.15}$$

where $p_0 = \eta^2/16$, and $p_c = \gamma^2\eta^2 e^{-4t_d\gamma_s}/4\,(2\gamma+2\,(\gamma^\star-2\gamma_s))^2$. There are totally four possible desired click events, so the success probability is $4p_0 = \eta^2/4$, and the fidelity is

$$F = \frac{1}{2} + \frac{p_c}{2p_0} = \frac{1}{2}(1 + \frac{\gamma^2 e^{-4t_d\gamma_s}}{(\gamma+2\gamma^\star-2\gamma_s)^2}). \tag{3.16}$$

Thus, similar to the result in the single-detection scheme, the indistinguishability limits the maximum of the fidelity, and the spin dephasing cause a time-dependent infidelity.

3.2 Entanglement connection schemes

In this section, we will discuss two scenarios and the corresponding entanglement connection scheme. Here the entanglement connection contains two aspects: entanglement swapping process and how the entanglement distance is extended in a scalable way. Still, we assume the quantum emitters are three-level systems as described in the previous section.

3.2.1 Nested scheme

In the scenario that the deterministic gate between the two memories in a repeater node is not possible and the nuclear spins are not accessible, the two-qubit gate can be mediated by photon, i.e., Bell-state measurement of the emitted photons, and the process can be scaled up via a nested scheme.

Entanglement swapping. Let us first label the four quantum emitters in the two links as 1, 2, 3, and 4, and the entanglement connection process starts with entangled state $\frac{1}{\sqrt{2}}(|\uparrow\downarrow\rangle + |\downarrow\uparrow\rangle)$ between emitter 1 and 2 as well as 3 and 4. The goal of entanglement connection is to entangle emitter 1 and 4, which requires performing measurements on the qubit state of 2 and 3.

Let us write down the joint state of four emitters

$$\frac{1}{2}(|\uparrow\downarrow\uparrow\downarrow\rangle + |\downarrow\uparrow\uparrow\downarrow\rangle + |\uparrow\downarrow\downarrow\uparrow\rangle + |\downarrow\uparrow\downarrow\uparrow\rangle). \tag{3.17}$$

We first apply the Barrett-Kok scheme on emitter 2 and 3, and this will eliminate the states $|\downarrow\uparrow\uparrow\downarrow\rangle$

and $|\uparrow\downarrow\downarrow\uparrow\rangle$ and result in state

$$\frac{1}{\sqrt{2}}(|\uparrow\downarrow\uparrow\downarrow\rangle + |\downarrow\uparrow\downarrow\uparrow\rangle). \tag{3.18}$$

Then a Hadamard gate is applied to both emitter 2 and 3, with resultant state

$$\frac{1}{\sqrt{2}}(|\uparrow -+\downarrow\rangle + |\downarrow +-\uparrow\rangle), \tag{3.19}$$

where $|+\rangle = (|\uparrow\rangle + |\downarrow\rangle)/\sqrt{2}$ and $|-\rangle = (|\uparrow\rangle - |\downarrow\rangle)/\sqrt{2}$. We can rewrite the state as

$$\frac{1}{2}\left[(|\uparrow_2\uparrow_3\rangle - |\downarrow_2\downarrow_3\rangle)\left(\frac{|\uparrow_1\downarrow_4\rangle + |\downarrow_1\uparrow_4\rangle}{\sqrt{2}}\right) + (|\uparrow_2\downarrow_3\rangle - |\downarrow_2\uparrow_3\rangle)\left(\frac{|\uparrow_1\downarrow_4\rangle - |\downarrow_1\uparrow_4\rangle}{\sqrt{2}}\right)\right]. \tag{3.20}$$

By measuring the spin state in emitter 2 and 3 the entanglement is successfully swapped. The resultant entangled state between emitter 1 and 4 can be determined by the measurement results: $(|\uparrow_1\downarrow_4\rangle + |\downarrow_1\uparrow_4\rangle)/\sqrt{2}$ for $|\uparrow_2\uparrow_3\rangle$ or $|\downarrow_2\downarrow_3\rangle$; $(|\uparrow_1\downarrow_4\rangle - |\downarrow_1\uparrow_4\rangle)/\sqrt{2}$ for $|\uparrow_2\downarrow_3\rangle$ or $|\downarrow_2\uparrow_3\rangle$.

Scalability. As the entanglement swapping process (basically Barrett-Kok scheme) is probabilistic, adopting a nested repeater structure would be the most efficient. The nested repeater scheme is shown in Fig. 3.1. In step (a), the entanglement is generated in each elementary link. Then, the entanglement swapping is processed at each nesting level. It is important to note that an unsuccessful entanglement swapping will destroy the state in the corresponding sublink, and the sublink should start over from step (a).

Repeater rates. Let us consider the scenario of a total distance L and 2^n repeater links where the nesting level is n. Starting from the elementary link, we consider an entanglement generation probability of p_0 and the case that entanglement is generated until the ith attempt, the probability density function (PDF) for i is thus

$$P(i) = p_0(1-p_0)^{i-1}. \tag{3.21}$$

The expectation value of i is $1/p_0$, and therefore the average time for a successful entanglement generation is $T_0\langle i\rangle = T_0/p_0$, where T_0 is the classical communication time.

Now let us consider the repeater with two links ($n = 1$), where the entanglement is generated independently with probability p_0 for each link. The entanglement swapping can be performed

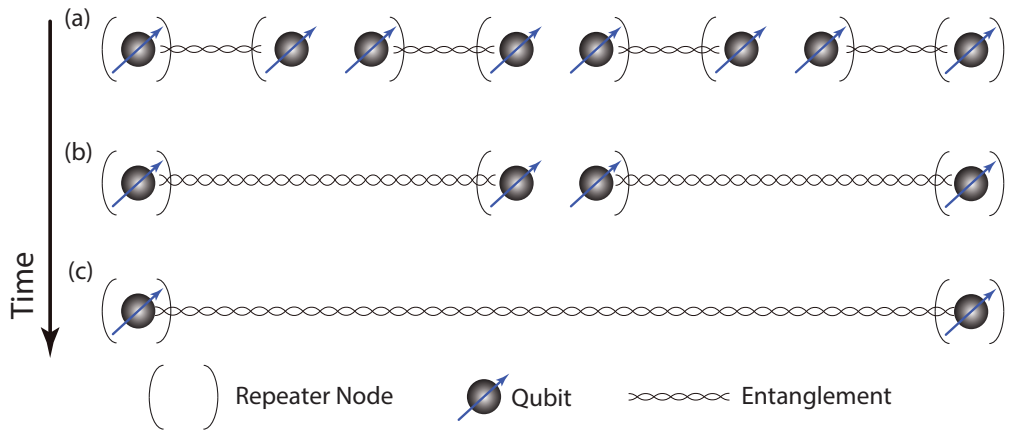

Figure 3.1: Schematic overview of the entanglement connection scheme with nested structure. Here is one example when nesting level is 2. Step (a) shows entanglement generation process in each elementary link. Step (b) and (c) shows entanglement swapping in the corresponding nesting level.

only after the entanglement is established in both links. We define variables i_1 and i_2 as the number of attempts to establish the two links, respectively, and thus the joint PDF for these two variables is $P_j(i_1,i_2) = p_0^2(1-p_0)^{i_1+i_2-2}$. We further define variable $i_{max} = \max\{i_1,i_2\}$, whose PDF is

$$P(i_{max}) = P(i_1 = i_{max}, i_2 < i_{max}) + P(i_1 < i_{max}, i_2 = i_{max}) + P(i_1 = i_{max}, i_2 = i_{max}). \tag{3.22}$$

The expectation value of i_{max} is calculated as $3/(2p_0)$. Taking the swapping probability p_s into account, the average time to distribute the entanglement across two links is $T_0\langle i_{max}\rangle/p_s = 3T_0/(2p_0p_s)$.

For higher nesting level, we can give a general formula for total entanglement distribution time

$$T_{tot} = T_0 \frac{f_1 f_2 \cdots f_n}{p_0 (p_s)^n}, \tag{3.23}$$

where the factor f_0 to f_n that satisfy $1 < f_i < 2$ are taken into account since for every kth level swapping attempt one has to establish two neighboring links at level $k-1$. This takes longer than establish a single such link by a factor f_i. We have calculated $f_1 = 3/2$, while no analytic expression for the rest factors is known so far [16]. It is suggested that $f_i = 3/2$ is a good estimation for all i [48]. Thus, we can rewrite the result in Eq. 3.23 as

$$T_{tot} = \left(\frac{3}{2}\right)^n \frac{T_0}{p_0 (p_s)^n}. \tag{3.24}$$

3.2.2 Non-nested scheme

In this section, we consider a single emitter with both electron spins and nuclear spins, a structure that is commonly seen in semiconductor quantum dots [49], defects in diamonds [50], and rare-earth-ions [44]. The deterministic two-qubit gate can be implemented between electron spin and nuclear spin via hyperfine interaction [51]. The nuclear spin has a long memory lifetime, but it can be accessed only through the interaction with the electron spin. Thus, in practice, the electron spins serve as communication qubits that create remote entanglement while nuclear spin store the entanglement.

In the case that the entanglement swapping process is probabilistic, a nested repeater scheme seems to be the optimal structure because the failure of the process will destroy the whole entangled state of the corresponding repeater chains. However, for the single emitter with both electron spin and nuclear spin, the electron spins are not storing the entanglement but mediate the entanglement generation, and thus the operation between remote electron spins will not disturb the entangled state in the nuclear spins. This means in the entanglement swapping process, it can be repeated many times until success while not affecting the entangled state, and thus a nested repeater structure is no longer necessary.

Entanglement swapping. Same as the previous section, we label the emitters and the process starts with the entangled state of electron spins between 1 and 2 as well as 3 and 4. The entanglement is then mapped to the corresponding nuclear spins by the operations illustrated in Fig. 3.2. The electron spins are initially entangled, and the corresponding nuclear spins are in state $(|\Uparrow\rangle + |\Downarrow\rangle)/\sqrt{2}$. A $C_e\text{NOT}_n$ gate, i.e., controlled-not gate with nuclear spin control electron spin, is applied to both emitters, followed by the measurement of the electron spin. Conditioned on the measurement, a Pauli X is applied to the second nuclear spin, and the entangled state is now stored in the nuclear spins.

After mapping the entanglement, the nuclear spin state is now

$$\frac{1}{2}(|\Uparrow_1\Downarrow_2\rangle + |\Downarrow_1\Uparrow_2\rangle) \otimes (|\Uparrow_3\Downarrow_4\rangle + |\Downarrow_3\Uparrow_4\rangle), \tag{3.25}$$

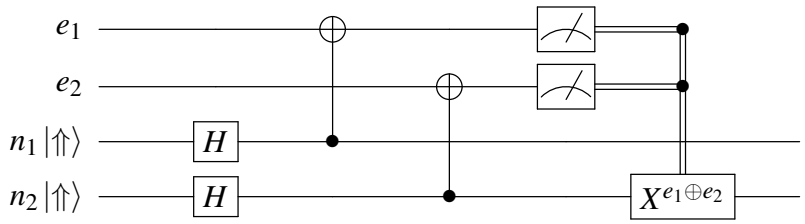

Figure 3.2: Quantum circuit illustration of the entanglement mapping process. The electron spin and nuclear spin are denoted as "e" and "n", respectively, with corresponding subscript that indicates the location. The electron spins initially stores the entangled state while the nuclear spins are prepared in state $(|\Uparrow\rangle + |\Downarrow\rangle)/\sqrt{2}$. The conditional gate $X^{e_1 \oplus e_2}$ is applied when $e_1 \oplus e_2 = 1$, i.e., the measurement results of electron spin 1 and 2 different.

and the electron spins are free. To swap the entanglement, one need to first entangle electron spin 2 and 3 using Barrett-Kok scheme. The remaining operation is illustrated by a quantum circuit, shown in Fig. 3.3. To begin with, one need to perform $\mathrm{C}_e\mathrm{NOT}_n$ in emitter 2 and 3. Then, the electron spins are measured in the Z basis, depending on which X gates may be applied to nuclear spin 3 and 4. Finally, nuclear spin 2 and 3 are measured in X basis, and the measurement result controls a Z gate on nuclear spin 4. One can check that the spin state after the operation is an entangled state of nuclear spin 1 and 4.

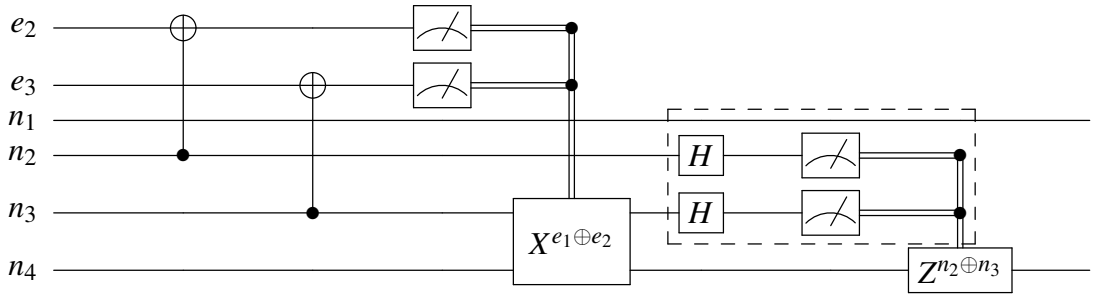

Figure 3.3: Quantum circuit representation of the entanglement swapping. The nuclear spins are first in state of Eq. 3.25, and the electron spins 2 and 3 are in entangled state $(|\uparrow_2\downarrow_3\rangle + |\downarrow_2\uparrow_3\rangle)/\sqrt{2}$. The dashed box represent the measurement of nuclear spin state, which can be done with the help of the electron spins.

As the direct readout of the nuclear spin is very challenging, one has to measure the nuclear spin mediated by the corresponding electron spins. The quantum circuit illustration is shown in Fig. 3.4.

Scalability The process can scale up without a nested structure. As we discussed in the pre-

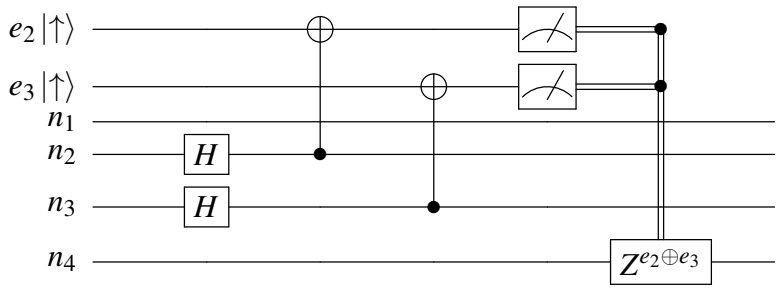

Figure 3.4: Quantum circuit illustration of readout with electron spins as ancillary qubits. This is equivalent to the circuit in the dashed box in FIG.3.3. Here the electron spins are initially in spin up, while the four nuclear spins are in GHZ-like state $\frac{1}{\sqrt{2}}(|\Uparrow_1\Downarrow_2\Uparrow_3\Downarrow_4\rangle + |\Downarrow_1\Uparrow_2\Downarrow_3\Uparrow_4\rangle)$. The Z gate on nuclear spin 4 are conditioned on the measurement result of electron spin 1 and 2. The result state of nuclear spin 1 and 4 is $\frac{1}{\sqrt{2}}(|\Uparrow_1\Downarrow_4\rangle + |\Downarrow_1\Uparrow_4\rangle)$.

vious section, the entanglement swapping has two stages: first, generate entanglement between electron spins in non-adjacent links, and map it to the corresponding nuclear spins; then generate entanglement between electron spins in the rest links and use it to assist the entanglement swapping process. This implies one can generate entanglement in the half links that are non-adjacent, and then generate entanglement in the rest links that are used to swap the entanglement. Based on this, we present a non-nested repeater structure, shown in Fig. 3.5.

Repeater rates. Let us consider the scenario of a total distance L and $2m$ repeater links. In the first step, the entanglement is generated in every second links (m links) simultaneously. Then, the entanglement is mapped to the nuclear spins and the remaining m links start generating entanglement. As all the process except the entanglement generation are deterministic, the total entanglement distribution time is

$$(\langle n^{(1)}_{max,m}\rangle + \langle n^{(2)}_{max,m}\rangle)\frac{L}{2mc} + T_m + T_s, \tag{3.26}$$

where $c = 2*10^8 \mathrm{ms}^{-1}$ is the speed of light in fiber, T_m is the entanglement mapping time, T_s is the entanglement swapping time, $n^{(1)}_{max,m}$ and $n^{(2)}_{max,m}$ are the total number of entanglement generation attempts to establish entanglement in all m links, i.e., $n_{max,m} = \max\{n_1, n_2, ..., n_m\}$ and here n_k is the number of attempts before successful entanglement generation in the k th link. Thus, the expectation value $\langle n^{(2)}_{max,m}\rangle = \langle n^{(1)}_{max,m}\rangle = \langle n_{max,m}\rangle$. For a single link, the probability of a successful entanglement generation with n trials is given in Eq. 3.21. Thus the joint probability of successful

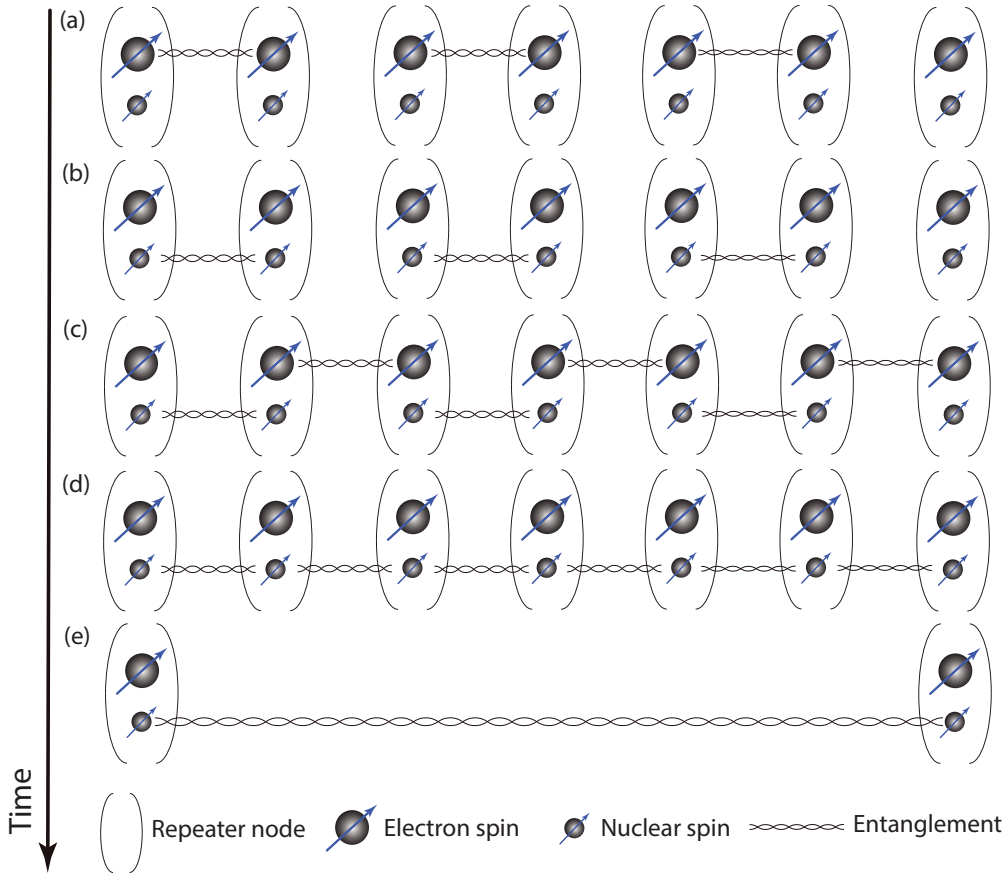

Figure 3.5: Schematic overview of the entanglement connection scheme with a non-nested structure. In step (a), the entanglement is generated in half of the links and is stored in the electron spin. Then the entanglement is mapped to the corresponding nuclear spin, while the electron spins are freed (step b). Next, the entanglement is generated in the rest links (step c) and mapped to the nuclear spin (step d). With measuring all the nuclear spins in between (mediated by the corresponding electron spin), the entanglement is successfully distributed (step e).

entanglement generation for all m links with attempts $n_1, n_2, ..., n_m$ is

$$P_j(n_1, n_2, ..., n_m) = \prod_{k=1}^{m} P(n_k) = p_0^m (1-p_0)^{\sum_{k=1}^{m} n_k - m}. \tag{3.27}$$

The probability distribution function of $n_{max,m}$ is

$$P(n_{max,m}) = \sum_{k=1}^{m} P_j(n_k = n_{max,m}, n_{\neq k} < n_{max,m}) + \sum_{k=1}^{l} \sum_{l=2}^{m} P_j(n_k = n_{max,m}, n_l = n_{max,m}, n_{\neq k \neq l} < n_{max,m})$$
$$+ ... + P_j(n_1 = n_2 = ... = n_m = n_{max,m}). \tag{3.28}$$

To calculate $\langle n_{max,m} \rangle$, let us simplify the problem by assuming $m = 2^n$. The PDF of $n_{max,m}$ can

Table 3.1: Numerical results of $k(n)$)

n	1	2	3	4	5
$k(n)$	1.5	2.08	2.72	3.38	4.05

be calculated using a iterative process

$$P_j(n_1,n_2) = P(n_1) * P(n_2)$$

$$P(n_{max,2}) = P_j(n_1 = n_{max,2}, n_2 < n_{max,2}) + P_j(n_1 < n_{max,2}, n_2 = n_{max,2})$$

...

$$P_j(n_{max1,2^k}, n_{max2,2^k}) = P(n_{max1,2^k}) * P(n_{max2,2^k})$$

$$P(n_{max,2^{k+1}}) = P_j(n_{max1,2^k} = n_{max,2^{k+1}}, n_{max2,2^k} < n_{max,2^{k+1}}) + P_j(n_{max1,2^k} < n_{max,2^{k+1}}, n_{max1,2^k} = n_{max,2^{k+1}}). \tag{3.29}$$

We define $\langle n_{max,2^n} \rangle = k(n)/p_0$,and the numerical result of $k(n)$ is given in Tab. 3.1. For example, $k(1) = 1.5$, which is the well-know $3/2$ relation [16]. The function $k(n)$ is almost linearly increase with n, and the regression result gives us

$$k(n) = 0.64n + 0.83. \tag{3.30}$$

Therefore, the average entanglement distribution time in Eq. 3.26 can be rewritten as

$$(0.64\log_2(m) + 0.83)\frac{L}{mcp_0} + T_m + T_s. \tag{3.31}$$

Chapter 4

Ensemble based quantum repeater protocols

4.1 DLCZ protocols

The DLCZ protocol is one of the first practical quantum repeater protocols using atomic ensembles as quantum memories. Different from the single emitter systems, atomic ensembles utilize the collective effects related to a large number of atoms in the ensemble, which allows a strong memory-photon interaction. This could greatly enhance the storage and retrieve efficiency, and therefore the entanglement generation rates [36, 52, 53]. The DLCZ protocol has inspired a large number of highly influential experiments [30, 54–61], showing that the approach of using atomic ensembles, linear optics, and photon counting is indeed very attractive from a practical point of view.

4.1.1 Protocol description

The basics of the DLCZ scheme is to generate photon-memory entanglement using a Raman-type quantum memory, which is ensemble of three-level systems with one exited state $|e\rangle$ and two ground states $|g_1\rangle$ and $|g_2\rangle$. Both $|g_1\rangle - |e\rangle$ and $|g_2\rangle - |e\rangle$ transition are permitted.

Memory-photon entanglement. To generate photon-memory entanglement, all the atoms are prepared in the ground state with lower energy, say $|g_1\rangle$. An off-resonant laser pulse on the $|g_1\rangle - |e\rangle$ transition leads to the spontaneous emission of a Raman photon on the $|e\rangle - |g_2\rangle$ emission. By convention, the emitted photon is denoted as "Stokes" photon. The process is shown as the "write process" of Fig. 4.1. Detection of the photon in the far field reveals no information about which atom it came from, and therefore creates an atomic state that is a coherent superposition of all

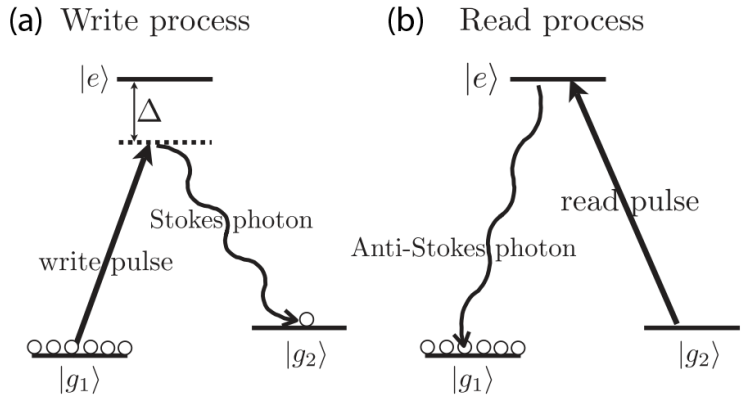

Figure 4.1: Illustration of the write (a) and read (b) process. Note in the write process, the write pulse is detuned from the transition frequency between $|g_1\rangle$ and $|e\rangle$.

possible state with one atom in $|g_2\rangle$ and the rest in $|g_1\rangle$

$$\frac{1}{N_A}\sum_{k=1}^{N_A} e^{i(\mathbf{k}_w-\mathbf{k}_S)\mathbf{x}_k}\,|g_1\rangle_1\,|g_1\rangle_2\ldots|g_2\rangle_k\ldots|g_1\rangle_{N_A}\,, \tag{4.1}$$

where $\mathbf{k}_w$ is the wave vector of the write laser, $\mathbf{k}_S$ is the wave vector of the detected Stokes photon, and $\mathbf{x}_k$ is the position of the kth atom. It is important to note that there is no collective interference, because each atom emits photon in random directions and the which-way information is stored in the atomic ensemble.

The collective excitation in 4.1 can be read out efficiently by converting it back to a single photon that propagates in a well defined direction. A read pulse on the $|g_2\rangle - |e\rangle$ transition is applied to the state, leading to an analogous state with one atom in $|e\rangle$ and the rest in $|g_1\rangle$. A supplementary phase $e^{i\mathbf{k}_r\mathbf{x}'_k}$, where $\mathbf{k}_S$ is the wave vector of the read laser and $\mathbf{x}_k$ is the position of the kth atom before read out, is added to the state. The excitation decays to the ground state and emit a photon on the $|e\rangle - |g_1\rangle$ transition (anti-Stokes photon). The amplitude for the photon to be emitted from the kth atom is proportional to

$$e^{i(\mathbf{k}_w-\mathbf{k}_S)\mathbf{x}_k}e^{i(\mathbf{k}_r-\mathbf{k}_{AS})\mathbf{x}'_k}, \tag{4.2}$$

where $\mathbf{k}_{AS}$ is the wave vector of the anti-Stokes photon. If the atoms are at rest between the write and the read process, i.e., $\mathbf{x}_k = \mathbf{x}'_k$, the constructive interference requires a phase matching condition

$\mathbf{k}_S + \mathbf{k}_{AS} = \mathbf{k}_w + \mathbf{k}_r$. This means the amplitude for photon that fulfill the condition is maximal and the direction of the anti-Stokes photon is predominantly by $\mathbf{k}_w + \mathbf{k}_r - \mathbf{k}_S$.

In the write process, an off-resonant write pulse is used to decrease the multi-photon emission. Let us analyze this process with the effective Hamiltonian

$$H = \chi(a^\dagger s^\dagger + as), \tag{4.3}$$

where χ is a coupling constant that is inverse propositional to the laser detuning Δ, $a^\dagger$ is the creation operator for a Stokes photon, and $s^\dagger$ is the creation operator for the superposition state Eq. 4.1. The Hamiltonian is equivalent to the Hamiltonian for parametric down-conversion process [62]. The state evolution can be derived using operator ordering techniques [63]

$$e^{-iHt}\left|0\right\rangle\left|0\right\rangle = \frac{1}{\cosh(\chi t)} e^{-i\tanh(\chi t)a^\dagger s^\dagger}\left|0\right\rangle\left|0\right\rangle = \frac{1}{\cosh(\chi t)}\sum_{m=0}^{\infty}(-i)^m \tanh^m(\chi t)\left|m\right\rangle\left|m\right\rangle, \tag{4.4}$$

where the state $\left|m\right\rangle\left|m\right\rangle$ represents m photons and m collective atomic excitations in $\left|g_2\right\rangle$, respectively. For small values of χt the expression can be expanded as

$$\left[(1-\frac{1}{2}(\chi t)^2)\right]\left|0\right\rangle\left|0\right\rangle - i\chi t\left|1\right\rangle\left|1\right\rangle - (\chi t)^2\left|2\right\rangle\left|2\right\rangle + O((\chi t)^3). \tag{4.5}$$

Thus, the probability of emitting one photon and two photons are $(\chi t)^2$ and $(\chi t)^4$, respectively. The emission of multiple photons will significantly decrease the state fidelity after the entanglement generation process, and therefore the one photon emission probability χt should be small to mitigate the error.

Entanglement generation. To generate entanglement between two remote memories A and B, both memories should first generate memory-photon entanglement, and then send the photons to the central beam-splitter, where a single-photon Bell-state measurement is performed. With a desired detector click, the state is

$$\left(1 + \sqrt{\frac{p}{2}}(s_a^\dagger a^\dagger e^{i\phi_a} + s_b^\dagger b^\dagger e^{i\phi_b}) + O(p)\right)\left|0\right\rangle, \tag{4.6}$$

where the subscript a and b denote the two memories, $a^\dagger$ and $b^\dagger$ represent the photon modes emitted by the two memories, ϕ_a and ϕ_b are the phases of the pump laser at two locations, and $\left|0\right\rangle$

is the vacuum state for all modes. After the single-photon Bell-state measurement, the state are projected to

$$|\psi_{ab}\rangle = \frac{1}{\sqrt{2}}(s_a^\dagger e^{i(\phi_a+\xi_a)} + s_b^\dagger e^{i(\phi_b+\xi_b)})\,|0\rangle\,, \tag{4.7}$$

where ξ_a and ξ_b are phases acquired by the photon in the corresponding channel. This state can ve rewritten as

$$|\psi_{ab}\rangle = \frac{1}{\sqrt{2}}(|1_a\rangle\,|0_b\rangle + |0_a\rangle\,|1_b\rangle\,e^{i\theta_{ab}}), \tag{4.8}$$

where $|0_{a/b}\rangle$ denotes an empty ensemble A/B, $|1_{a/b}\rangle$ denotes the state with a single excitation, and $\theta_{ab} = \phi_b - \phi_a + \xi_b - \xi_a$ is the relative phase. The success probability for the entanglement generation process is $p_0 = p\eta_d\eta_t$, where $p = (\chi t)^2$ is the probability of emitting a single photon, η_d is the detector efficiency, and $\eta_t = \exp(-L_0/2L_{att})$ is the transmission efficiency corresponding a distance of $L_0/2$ and fiber attenuation length L_{att} (a typical value is 22 km for optimal wavelength).

Entanglement connection. Let us consider two links AB and CD with B and C in the same node, where entanglement has been generated independently in both links. The entanglement swapping requires to read out the atomic excitation that are probabilistically stored in the ensembles B and C. The single-photon Bell-state measurement is performed on the possible emitted photon, and a single click will result in the state

$$|\psi_{ad}\rangle = \frac{1}{\sqrt{2}}(|1_a\rangle\,|0_d\rangle + |0_a\rangle\,|1_d\rangle\,e^{i(\theta_{ab}+\theta_{cd})}). \tag{4.9}$$

In the case that the detector efficiency η_d and memory efficiency η_m are not unity, or the detector cannot resolve photon number, the detector may also give expected click when two photons are emitted while one of them is lost during transmission. This will create a vacuum component

$$\rho_{ad} = \alpha^{(1)}\,|\psi_{ad}\rangle\,\langle\psi_{ad}| + \beta^{(1)}\,|0\rangle\,\langle 0|\,, \tag{4.10}$$

where $\alpha^{(1)} = 1/(2-\eta)$ is the fidelity of the state, $\beta^{(1)} = (1-\eta)/(2-\eta)$, and $\eta = \eta_m\eta_d$. The success probability for the first swapping is $p_s^{(1)} = \eta(1-\eta/2)$.

The entanglement swapping at higher nesting level follows the same procedure. The fidelity of the state in the next nesting level and the swapping probability depend on the fidelity of the state

in the present nesting level. Consider the state of two links before swapping

$$\begin{aligned}\rho_1 &= \alpha_1 |\psi_1\rangle \langle\psi_1| + (1-\alpha_1)\rho_1' \\ \rho_2 &= \alpha_2 |\psi_2\rangle \langle\psi_2| + (1-\alpha_2)\rho_2',\end{aligned} \tag{4.11}$$

where $|\psi_1\rangle$ and $|\psi_2\rangle$ are the entangled state and ρ_1', ρ_2' are the unwanted state. After swapping, the new state can be expressed as

$$\rho = \alpha |\psi_{12}\rangle \langle\psi_{12}| + (1-\alpha)\rho', \tag{4.12}$$

where $|\psi_{12}\rangle$ is the entangled state determined by the Bell-state measurement, and ρ' is the unwanted state. Single-photon BSM will keep creating vacuum states since it cannot exclude the situation where the two photons are stored in the two local nodes in neighboring links. Therefore, the fidelity of resultant state α is

$$\alpha = \frac{\alpha_1 \alpha_2}{\alpha_1 + \alpha_2 - \alpha_1 \alpha_2 \eta_p}, \tag{4.13}$$

and the success probability is

$$p_s = \frac{1}{2}(\alpha_1 \eta_p + \alpha_2 \eta_p - \alpha_1 \alpha_2 \eta_p^2), \tag{4.14}$$

where η_p is the probability that a photon can be retrieved and detected. For DLCZ scheme $\eta_p = \eta = \eta_m \eta_d$.

To calculate the probability and the fidelity for higher nesting level, it is valid to assume $\alpha_1 = \alpha_2 = \alpha^{(i)}$, and thus

$$\alpha^{(i+1)} = \frac{\alpha^{(i)}}{2 - \alpha^{(i)}\eta}, \tag{4.15}$$

and

$$p_s^{(i+1)} = \alpha^{(i)} \eta \left(1 - \frac{\alpha^{(i)}\eta}{2}\right), \tag{4.16}$$

with $p_s^{(1)} = \eta\,(1 - \eta/2)$.

Postselection. It is important to note that single-photon BSM requires qubits to be encoded as the collective excitation state (photon number state), which cannot be used directly for quantum

Figure 4.2: Sketch of the postselection process. Entanglement has been independently distributed in both link. For both ends the atomic excitations are read out, and single-photon BSMs are performed.

communication tasks, and thus postselection is necessary to convert the qubits into a useful two-photon entangled state analogous to qubit states in two-photon BSM [16]. The process is shown in Fig. 4.2. Entanglement is first generated independently in two links with the same spacial location. Then the atomic excitations are read out for both ends of the links, and for each end, the photon is retrieved, resulting state

$$|\psi_{az}\rangle = \frac{1}{\sqrt{2}}(a_1'^{\dagger} z_2'^{\dagger} + e^{i(\theta_2-\theta_1)} a_2'^{\dagger} z_1'^{\dagger})\,|0\rangle\,, \tag{4.17}$$

where $a_{1/2}'^{\dagger}$ and $z_{1/2}'^{\dagger}$ are photon mode in the corresponding channel, and θ_1 and θ_2 are the phases acquired in $A_1 - Z_1$ and $A_2 - Z_2$ link, respectively. The state is analogous to a conventional polarization or time-bin entangled state. Measurements in arbitrary basis are possible by combining modes in the same location in a beam-splitter followed by a photon detection. The probability of the postselection process is $p_{ps} = (\alpha^{(n)}\eta)^2/2$, where the one half is the intrinsic probability of two-photon Bell-state measurement.

4.1.2 Entanglement distribution time

The total entanglement distribution time for the DLCZ scheme is

$$T_{tot} = \frac{L_0}{c}\frac{f_0 f_1 \cdots f_n}{p_0 p_s^{(1)} \cdots p_s^{(n)} p_{ps}}, \tag{4.18}$$

where as we mentioned in the previous chapter, f_i is the extra factor required to generate entanglement in both link of ith nesting level and $3/2$ is a good approximation. Substituting Eq. 4.15 and

Eq. 4.16, we can rewrite the total time as

$$T_{tot} = 3^{n+1} \frac{L_0}{c} \frac{\prod_{k=0}^{n} (2^k - (2^k - 1)\eta)}{\eta_d \eta_t p \eta^{n+2}}. \tag{4.19}$$

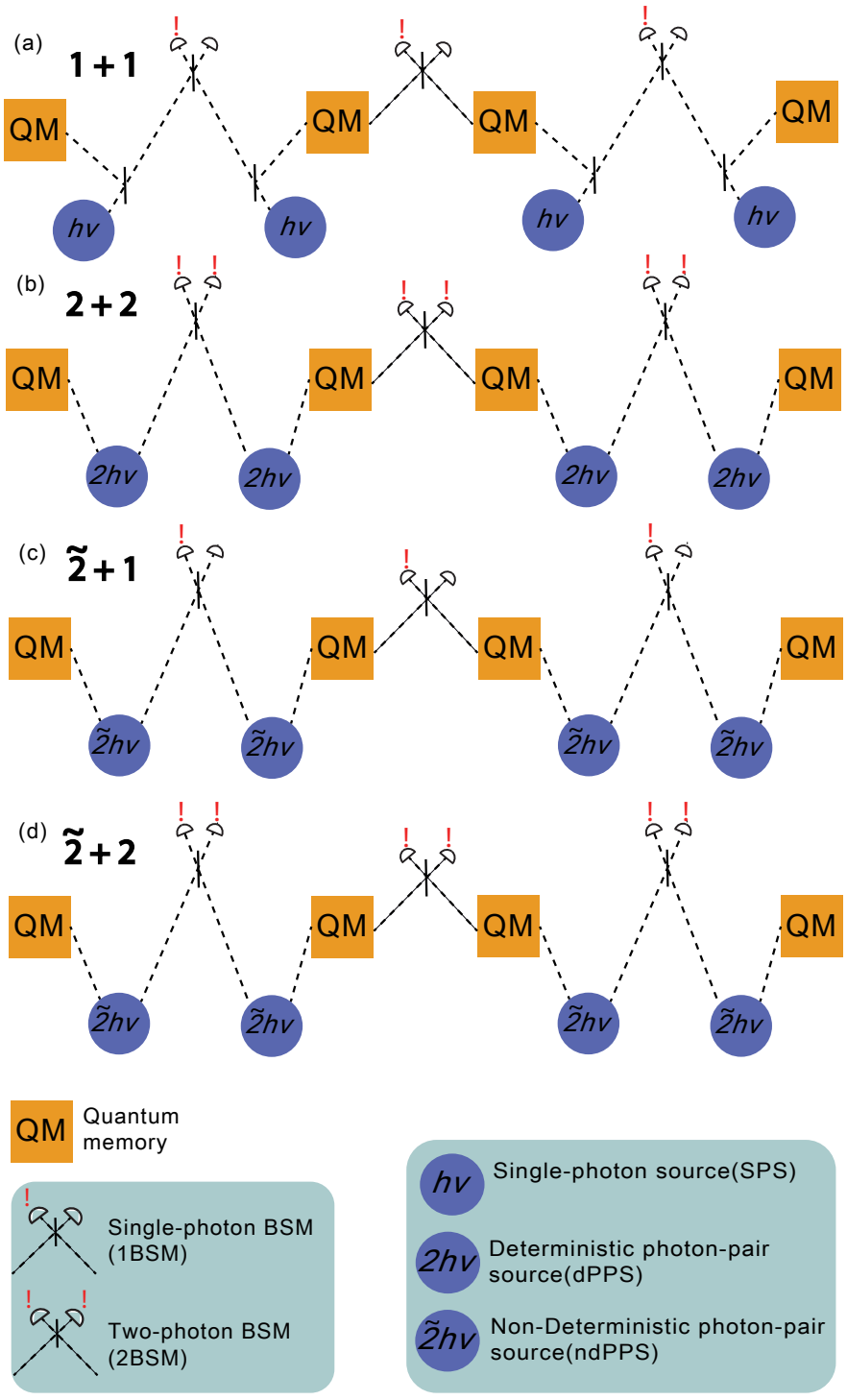

Figure 4.3: Sketches of quantum repeater protocols we mainly discuss in this paper. Here we show the two-link version of these repeater protocols. (a)Single-photon source(SPS) with single-photon BSM ("1 + 1"). (b)Deterministic photon-pair source(dPPS) with two-photon BSM ("2 + 2"). (c)Non-deterministic photon-pair source(ndPPS) with single-photon BSM ("$\tilde{2}$ + 1"). (d) Non-deterministic photon-pair source(ndPPS) with two-photon BSM ("$\tilde{2}$ + 2").

4.2 Improved protocols

Though the DLCZ scheme has attracted broad interest, its limitations are also obvious. To begin with, in the entanglement generation process, the single-photon emission probability must be small to reduce multi-photon emission, which severely limits the repeater rates. Besides, the entanglement distribution requires interferometric stability over long distances. Moreover, the wavelength of the Stokes photon has to be in the telecom-wavelength range (around 1.5 μm) to minimize the photon loss, which greatly restricts the choices of the atomic ensemble without frequency conversion.

Many improved protocols were proposed to mitigate these issues by separating memory and photon source [48, 64–69]. In this thesis, we will focus on four of them, namely, scheme with single-photon sources and single-photon Bell-state measurements [64], scheme with deterministic photon-pair sources and two-photon Bell-state measurements [68], and scheme with non-deterministic photon-pair sources and single-photon [65] or two-photon [69] Bell-state measurements. The schemes are shown in Fig. 4.3.

4.2.1 Single-photon source(SPS) with single-photon BSM scheme ("1 + 1")

Entanglement generation. The "1 + 1" protocol uses deterministic single-photon sources at each node. A single photon is generated in each node and sent through a local beam-splitter, after which is with probability γ stored in a quantum memory and with probability $1-\gamma$ injected to the central interferometer. The quantum state with photon modes is (with $a_i^\dagger$ becomes $s_i^\dagger$)

$$(\sqrt{1-\gamma}a_1'^\dagger + \sqrt{\gamma}a_1^\dagger) \otimes (\sqrt{1-\gamma}a_2'^\dagger + \sqrt{\gamma}a_2^\dagger)\,|0\rangle\,, \tag{4.20}$$

where $a^\dagger$ and $a'^\dagger$ represent the creation operator of photon mode transmitted (send to central beam-splitter) and reflected (send to qauntum memory), respectively. As the central beam splitter erases the which-path information, the successful detection of a single-photon in the central station will

create an entangled photon number state of two memories

$$|\psi_{ab}\rangle = \frac{1}{\sqrt{2}}(s_1^\dagger + s_2^\dagger)|0\rangle, \tag{4.21}$$

where $s^\dagger$ is the creation operator of memory state with single atomic excitation.

In the presence of photon loss and non-unity quantum memory efficiency, a vacuum component is created during the process, resulting in the state

$$(1-\gamma)|\psi_{ab}\rangle\langle\psi_{ab}| + \gamma|0\rangle\langle 0|, \tag{4.22}$$

and the success probability is $p_0 = 2\eta_s\gamma\eta_t\eta$, where η_s is the single-photon source efficiency. Here we have considered the memory efficiency which is the product of storage efficiency and retrieval efficiency, in the entanglement generation process.

Entanglement swapping, postselection and entanglement distribution time. The entanglement swapping follows the same process as in the DLCZ process and the entanglement swapping probability can be calculated using Eq. 4.15 and Eq. 4.16. Here the swapping probability for the first nesting level is $p_s^{(1)} = (1-\gamma)\eta\,[1-(1-\gamma)\eta/2]$. Postselection is also necessary with probability $p_{ps} = (\alpha^{(n)}\eta)^2/2$.

One can show that the total entanglement distribution time for a repeater link a nesting level n is

$$T_{tot} = \frac{3^{n+1}}{2}\frac{L_0}{c}\frac{\prod_{k=0}^{n}(2^k-(2^k-1)\eta_s(1-\gamma)\eta)}{\eta_d\eta_t\eta_s^{n+3}\gamma(1-\gamma)^{n+2}\eta^{n+2}}. \tag{4.23}$$

4.2.2 Deterministic photon-pair source(dPPS) with two-photon BSM ("2 + 2")

Entanglement generation. The protocol uses deterministic entangled photon-pair sources that emit a photon-pair, where one photon is sent to a quantum memory and the other one to a central station, respectively. Depending on the qubit encoding(time-bin, frequency, polarization, etc), the two-photon BSM will project the two quantum memories into an entangled state in the corresponding space. Take polarization photon-pair source as an example: the source emits a pair of photon that are of same polarization, and one photon is stored by the quantum memory and the other is

sent to a central beam-splitter. The state can be expressed as

$$\frac{1}{\sqrt{2}}(a'^{\dagger}_{1H}a^{\dagger}_{1H}+a'^{\dagger}_{1V}a^{\dagger}_{1V})\otimes\frac{1}{\sqrt{2}}(a'^{\dagger}_{2H}a^{\dagger}_{2H}+a'^{\dagger}_{2V}a^{\dagger}_{2V})\,|0\rangle\,, \tag{4.24}$$

where H and V represent horizontal and vertical polarization, and $a'^{\dagger}_{H/V}$ and $a^{\dagger}_{H/V}$ are creation operators of photon modes with horizontal/vertical polarization that are sent to the memory and central beam-splitter, respectively. After two-photon Bell-state measurement, the final state depends on the BSM result, and one example is

$$|\psi\rangle_{ab}=\frac{1}{\sqrt{2}}(s^{\dagger}_{1H}s^{\dagger}_{2V}+s^{\dagger}_{1V}s^{\dagger}_{2H})\,|0\rangle\,. \tag{4.25}$$

The success probability for an desired detector click is $p_0=\eta_t^2\eta_s^2\eta^2/2$, where the one half is due to the intrinsic probability of two-photon Bell-state measurement.

It is important to note the fidelity of this scheme is robust against photon loss as it will not give the desired detector click. Besides, the photon sources do not require phase stabilization of the linear interferometer [70]. Moreover, the photon-pair source can have a different frequency in the two arms, and it is not hard to tune one of them to match the telecom frequency while another match the transition frequency of the memory. Therefore, one has more flexible choices of quantum memories in terms of transition frequency.

Entanglement swapping and entanglement distribution time. In the entanglement swapping process, the photons stored in the local quantum memories are retrieved and sent to the Bell-state measurement station. As the entanglement swapping produce no vacuum state, the swapping probability at any nesting level is $p_s^{(i)}=\eta^2/2$. Postselection is no longer necessary. Therefore, the total entanglement distribution time is

$$T_{tot}=3^n\frac{L_0}{c}\frac{2}{\eta_t^2\eta_s^2\eta^{n+2}}. \tag{4.26}$$

4.2.3 Non-deterministic photon-pair source (ndPPS) with single-photon BSM scheme ("$\tilde{2}$ + 1")

The ndPPS emits photon-pair probabilistically, with one photon stored in the quantum memory and another sent to the central station. As for the "1 + 1" scheme, a successful single-photon

BSM will project the two memories into the entangled photon number state. Similarly to the DLCZ scheme [36], the emission probability should be small to suppress multi-pair emission. The success probability of entanglement generation is $p_0 = 2\eta_t\eta_s\eta$, and the state created is the same as the state generated in the DLCZ scheme (Eq. 4.10). The entanglement swapping and postselection process are also the same as DLCZ scheme, and thus the total entanglement distribution time is

$$T_{tot} = 3^{n+1}\frac{L_0}{c}\frac{\prod_{k=0}^{n}(2^k-(2^k-1)\eta)}{\eta_d\eta_t\eta_s\eta^{n+2}}, \tag{4.27}$$

where η_s is the probability of emitting a photon-pair for non-deterministic photon source. It is important to notice that in the "1 + 1" and "2 + 2" scheme we have defined source efficiency η_s, which refers to the probability to extract a photon in deterministic photon source. In this paper, we do not distinguish these two terms and call them "source efficiency" η_s.

4.2.4 Non-deterministic photon-pair source (ndPPS) with two-photon BSM scheme ("$\tilde{2}$ + 2")

This scheme is similar to the "2 + 2" scheme while using non-deterministic entangled photon-pair sources. It is possible, albeit with small probability, to get coincident photon-pair emission from two ndPPS. The successful two-photon BSM will project the two memories into the two-photon entangled state. Again the multi-pair emission probability has to be kept small; the associated errors can be mitigated by appropriately designed entanglement swapping [67] and photon-number resolving detection [69]. The total entanglement distribution time is

$$T_{tot} = 3^{n}\frac{L_0}{c}\frac{2}{\eta_t^2\eta_s^2\eta^{n+2}}, \tag{4.28}$$

which is the same as Eq. 4.26, however, with the difference that the source efficiency η_s here is much smaller.

4.3 Comparison of repeater rates

We plot the comparison of repeater rates for these four schemes and the case of direct transmission, shown in Fig. 4.4. The parameters used here considered high memory efficiency and infinite mem-

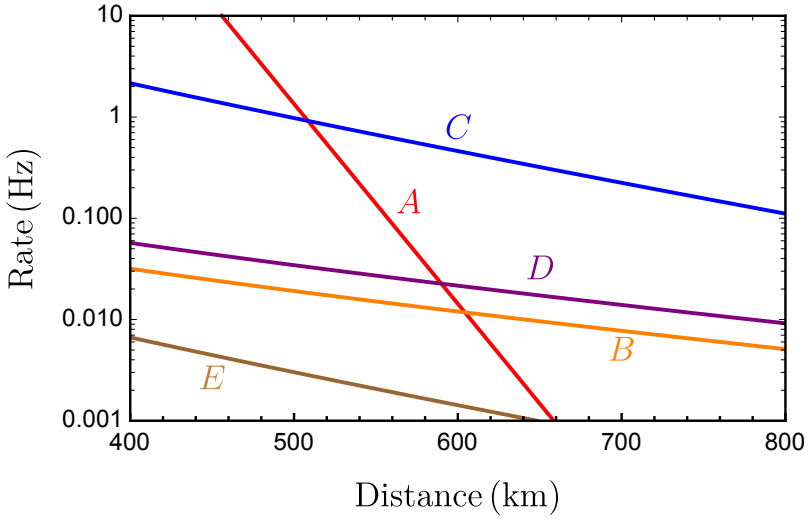

Figure 4.4: Comparison of repeater rates for various quantum repeater protocols: (A): direct transmission of photons through optical fiber with single-photon generation rate of 10 GHz as a reference; (B): the "1 + 1" scheme; (C): the "2 + 2" scheme; (D): the "$\tilde{2}$ + 1" scheme; (E): the "$\tilde{2}$ + 2" scheme. The plots are for 8 elementary links, corresponding nesting level 3. The parameters used are memory efficiency and detector efficiency $\eta_m = \eta_d = 0.9$, fiber attenuation distance $L_{att} = 22$ km, local beam-splitter transmission probability $\gamma = 0.16$ for the "1 + 1" scheme, $\eta_s = 0.9$ for the "1 + 1" scheme and the "2 + 2" scheme, $\eta_s = 0.05$ for the "$\tilde{2}$ + 1" scheme and the "$\tilde{2}$ + 2" scheme.

ory lifetime. The four schemes outperform direct transmission at 510 km (the "2 + 2" scheme), 590 km (the "$\tilde{2}$ + 2" scheme), 600 km (the "1 + 1" scheme), and 660 km (the "$\tilde{1}$ + 1" scheme), respectively. The two-photon BSM scheme outperforms the corresponding single-photon BSM scheme though the entanglement generation probability is much smaller. This is because the post-selection process is not required for the two-photon BSM schemes, and time saved surpasses the impact of smaller entanglement generation probability. The schemes with deterministic photon source have higher repeater rates than the corresponding non-deterministic photon source due to the higher source efficiency and therefore higher entanglement generation probability.

Chapter 5

Near-term repeater performance for ensemble based quantum memories

There has recently been significant experimental progress in the entanglement of two remote quantum memories (corresponding to one repeater link) [22, 30, 71–73]. For example, Ref. [30] demonstrated entanglement between two ^{87}Rb atomic ensembles separated by 22 km of coiled fiber. Simple repeater demonstrations with two links, however, have not been reported yet. The main limitation is the imperfect quantum devices, especially short memory lifetime. It is therefore important to make realistic theoretical predictions for such demonstrations. In this thesis, we consider a near-term case of two repeater links with finite quantum memories. We have developed a unified approach to estimate the repeater rates with imperfect quantum memories for different repeater protocols. Our results suggest that such demonstrations are within reach of current technology. This work has been published in PRA [29].

5.1 Mathematical derivation

Previous papers have studied the performance of repeaters with imperfect ensemble-based memories [16, 68, 69, 74–77], but they have typically either focused on more long-term scenarios and made assumptions that are not quite realistic yet, such as a high degree of multiplexing, or have made idealizations that may affect quantitative rate predictions, such as a simple cut-off for the storage time, rather than an exponential decay. Decoherence in ensemble-based memories results in a reduction of efficiency rather than fidelity [27]. While this is positive from the point of achieving high final-state fidelity in quantum repeater protocols, it complicates the derivation of accurate repeater rates because it makes the swapping probabilities time-dependent.

5.1.1 General framework of rates calculation

Two-link situation. Let us first recall the basic probability distribution functions (PDFs) associated with repeater rates calculation. For an elementary link, one has to try many times until the entanglement is successfully generated. After each attempt, one has to wait for the Bell-state measurement signal that tells whether the attempt is successful. If not, the memories need to be emptied and one needs to try again. In this paper, we do not consider the time of memory reinitialization (which is typically negligible compared with communication time) and thus the time required for each attempt is $T_0 = L_0/c$, where L_0 is the length of an elementary link and $c = 2 * 10^8$ ms^{-1} is the speed of light in an optical fiber. Considering an entanglement generation probability of p_0 and the case that entanglement is generated until the nth attempt, the PDF for n is

$$P(n) = p_0(1-p_0)^{n-1}. \tag{5.1}$$

We do not consider the dark counts of the detectors since they can be vary small. Superconducting nanowire single-photon detectors with a 30Hz dark count rate are already used in measurement-device-independent quantum key distribution [21], and milli-Hz dark count rate has also been demonstrated [78].

Now let us consider the repeater with two links, where the entanglement is generated independently with probability p_0 for each link. The entanglement swapping can be performed only after the entanglement is established in both links. We define variables n_1 and n_2 as the number of attempts to establish the two links, respectively, and thus the joint PDF for these two variables is $P(n_1,n_2) = p_0^2(1-p_0)^{n_1+n_2-2}$. We further define three variables n_{max}, n_{min}, and n_{dif}, denoting $\max\{n_1,n_2\}$, $\min\{n_1,n_2\}$ and $|n_1-n_2|$, respectively. Obviously, they are related by $n_{max} = n_{min} + n_{dif}$. It is useful to show the probability distribution function of n_{dif}

$$p(n_{dif}) = \begin{cases} \dfrac{2p_0(1-p_0)^{n_{dif}}}{2-p_0} & n_{dif} \neq 0 \\ \dfrac{p_0}{2-p_0} & n_{dif} = 0 \end{cases} \tag{5.2}$$

and the expectation of these variables

$$\begin{aligned}\langle n_{max}\rangle &= \frac{3-2p_0}{(2-p_0)p_0}; \langle n_{min}\rangle = \frac{1}{(2-p_0)p_0} \\ \langle n_{dif}\rangle &= \frac{2-2p_0}{(2-p_0)p_0}.\end{aligned} \tag{5.3}$$

We call $n_{max}T_0$ the "preparation time", and $n_{dif}T_0$ the "decay time"(waiting time). This is to say, the entanglement swapping is performed after the preparation time, and the entangled state of one link is destroyed during the decay time. The memory decay, which will not decrease the fidelity but the efficiency [27], is modeled as the following general situation

$$\begin{aligned}&\alpha\left|\Psi\right\rangle\left\langle\Psi\right| + (1-\alpha)\rho \xrightarrow{decay} \\ &e^{-\Delta t/\tau_m}\alpha\left|\Psi\right\rangle\left\langle\Psi\right| + (1-e^{-\Delta t/\tau_m}\alpha)\rho',\end{aligned} \tag{5.4}$$

where $\left|\Psi\right\rangle\left\langle\Psi\right|$ represents the maximized entangled state that we are interested in, ρ and ρ' are "unwanted states" that have no contribution to the repeater performance, and Δt and τ_m are the decay time and the lifetime of the memory, respectively. It is important to notice that the "efficiency" mentioned above is actually $\eta_m e^{-\Delta t/\tau_m}$, where η_m is the efficiency of quantum memory without decay. To make a clear distinction between memory efficiency and lifetime, we call η_m the memory efficiency in the text.

The decay time in Eq. (5.4) is the waiting time for the single-photon BSM, while it is two times the waiting time for two-photon BSM since both memories in a link will decay. The entanglement swapping probability p_s and resultant state, therefore, depend on the decay time, and thus n_{dif}. This dependence can be understood via the following calculation: before swapping, one has to establish two neighboring links, which could not be perfect and thus we consider two mixed states

$$\begin{aligned}\rho_1 &= \alpha_1\left|\Psi_1\right\rangle\left\langle\Psi_1\right| + (1-\alpha_1)\rho_1 \\ \rho_2 &= \alpha_2\left|\Psi_2\right\rangle\left\langle\Psi_2\right| + (1-\alpha_2)\rho_2,\end{aligned} \tag{5.5}$$

where $\left|\Psi_1\right\rangle$ and $\left|\Psi_2\right\rangle$ are the entangled state and ρ_1, ρ_2 are the unwanted state. After swapping, the new state can be expressed as

$$\rho = \alpha\left|\Psi_{12}\right\rangle\left\langle\Psi_{12}\right| + (1-\alpha)\rho, \tag{5.6}$$

where $|\Psi_{12}\rangle$ is the entangled state determined by the Bell-state measurement, and ρ is the unwanted state. It is important to notice that the unwanted state in the single-photon BSM is a pure vacuum state, while in two-photon BSM it contains the resultant states from both single-memory decay and two-memory decay(vacuum state). For the two-photon BSM, the swapping will eliminate all other cases than the entangled state. The expression of α and the success probability p_s, depend on the type of Bell-state measurement(BSM). Single-photon BSM will create a vacuum state since it cannot exclude the situation where the two photons are stored in the two local nodes in neighboring links. Therefore, the fidelity of resultant state α is

$$\alpha = \frac{\alpha_1 \alpha_2}{\alpha_1 + \alpha_2 - \alpha_1 \alpha_2 \eta_d}, \tag{5.7}$$

and the success probability is

$$p_s = \frac{1}{2}(\alpha_1 \eta_d + \alpha_2 \eta_d - \alpha_1 \alpha_2 \eta_d^2), \tag{5.8}$$

where η_d is the detector efficiency. It is important to note that the definition of fidelity and success probability is different from the definition in Ref. [16], where we substitute the product of detector efficiency and memory efficiency $\eta_d \eta_m$ with only detector efficiency η_d. This is because we will consider the memory efficiency in the entanglement generation process, where an unsuccessful storage or retrieval of the photon will create a vacuum state, and thus α_1 and α_2 depend on the memory efficiency.

On the other hand, the resultant state of two-photon BSM is a pure entangled state and thus the fidelity is

$$\alpha = 1. \tag{5.9}$$

The success probability is simply

$$p_s = \alpha_1 \alpha_2 \eta_d^2 / 2, \tag{5.10}$$

where the half is the intrinsic success probability of usual two-photon BSM.

In the entanglement swapping process, if the first link establishes the entanglement first, the memory in this link would decay and thus $\alpha_1 = \alpha_0 \exp(-n_{dif} T_0 / \tau_m)$, $\alpha_2 = \alpha_0$, where α_0 is the

entangled state fidelity after entanglement generation. Therefore, the swapping probability in both case, and the state fidelity after swapping in the single-photon BSM situation depend on n_{dif}.

Now let us calculate the average entanglement distribution time(EDT) for the two-link situation. Without loss of generality, we consider a successful entanglement swapping after rth swapping attempts and the EDT for this case is given by the following expression:

$$T_{tot}^{(1)} = \sum_{k=1}^{\infty} [(\sum_{r=1}^{k} n_{r,max} T_0) p_{k,s} \prod_{r=1}^{k-1} (1 - p_{r,s})], \tag{5.11}$$

where the subscript "k" denotes the kth swapping attempt, and therefore $\sum_{k=1}^{r} n_{k,max} T_0$ is the total preparation time in total r swapping attempts and $p_{r,s} \prod_{k'=1}^{r-1} (1 - p_{k',s})$ is the corresponding probability. The expectation of the EDT also requires averaging $n_{k,max}$, and $n_{k,dif}$, which is difficult since both $p_{k,s}$ and $n_{k,max}$ depend on $n_{k,dif}$. It is easier to rewrite $n_{k,max}$ as $n_{k,dif} + n_{k,min}$, where $n_{k,min}$ is independent of $n_{k,dif}$. It is however, still difficult to calculate analytically the result without assumptions on $\langle n_{k,dif} * p_{k,s} \rangle$, where $p_{k,s}$ depends on the waiting time and therefore on $n_{k,dif}$. We define a new variable $\beta = \langle n_{k,dif} * p_{k,s} \rangle / \langle n_{k,dif} \rangle \langle p_{k,s} \rangle$, and clearly, we have

$$0 < \beta < 1, \tag{5.12}$$

where the right side "$<$" is because $n_{k,dif}$ and $p_{k,s}$ are negatively correlated. The numerical evidence discussed in Appendix B suggests that in single-photon BSM,

$$\beta \approx 1. \tag{5.13}$$

On the other hand, in the two-photon BSM, β can reach lower bound and upper bound in Eq. (5.12) in different regimes: in the low-p_0 regime, $\beta \approx 1$, while in the high-p_0, high-lifetime regime, $\beta \approx 0$.

With Eq. (5.13) and Eq. (5.12), we can simplify Eq. (5.11)

$$\langle T_{1tot}^{(1)} \rangle = \frac{1}{\langle p_s \rangle} (\langle n_{dif} \rangle + \langle n_{min} \rangle) T_0 = \frac{\langle n_{max} \rangle}{\langle p_s \rangle} T_0, \tag{5.14}$$

for single-photon BSM and

$$\frac{\langle n_{min} \rangle}{\langle p_s \rangle} T_0 < \langle T_{2tot}^{(1)} \rangle < \frac{\langle n_{max} \rangle}{\langle p_s \rangle} T_0. \tag{5.15}$$

for two-photon BSM, where the detailed derivation can also be found in Appendix A. It is important to notice that for two-photon BSM, $T_{2tot}^{(2)}$ can be estimated using the average of the lower and upper bound $(\langle n_{min}\rangle T_0/\langle p_s\rangle + \langle n_{max}\rangle T_0/\langle p_s\rangle)/2 = T_0/p_0\langle p_s\rangle$. As we can see from Eq. (5.3), in the worst case $\langle n_{max}\rangle$ is no more than $3\langle n_{min}\rangle$, and the error rate of this estimation is thus no more than 50%, which is still a good estimation since repeater rates vary over many orders of magnitude.

Postselection and beyond two links. Though we have given the EDT for repeater schemes with single-photon BSM in Eq. (5.14), the entanglement is imperfect and cannot be used directly for quantum communication purpose and thus postselection is necessary. To implement postselection, a separate chain of two links is placed in such a way that the two end nodes are placed at the same location as the two end nodes from the original chain, respectively. After entanglement is established in both chains, single-photon BSM is performed at each end and the state is projected into a two-photon entanglement state [36]. The treatment of the postselection is analog to the four-link situation(nesting level of 2). It is important to note that the EDT beyond two links is interesting in general, even if our motivation here is to include postselection.

We consider the establishment times T_1 and T_2, and state fidelities α_1 and α_2, respectively for two sublinks. The average establishment time and the state fidelity are given in Eq. (5.14) and Eq. (5.7). Here we follow the same procedure in the two-link situation and consider the postselection is successful at the jth attempt. The EDT is expressed as

$$T_{tot}^{(2)} = (\sum_{i=1}^{j} T_{i,max}) p_{j,ps} \prod_{i'=1}^{j-1} (1 - p_{i',ps}), \tag{5.16}$$

where the subscript "i" represent the ith postselection attempt, $p_{i,ps} = \alpha_{i,1}\alpha_{i,2}\exp(-T_{i,dif}r)$ is the postselection probability for ith attempt, $T_{i,max} = \max\{T_{i,1}, T_{i,2}\}$, and $T_{i,dif} = |T_{i,1} - T_{i,2}|$. Hence, $\sum_{i=1}^{j} T_{i,max}$ is the total time for a success in the jth postselection attempt and $p_{j,ps}\prod_{i'=1}^{j-1}(1 - p_{i',ps})$ is the corresponding probability. The calculation also requires averaging j, $T_{i,max}$ and $T_{i,dif}$, which is difficult since both $T_{i,max}$ and $p_{i,ps}$ depend on $T_{i,dif}$ and we do not know the exact probability distribution function. Fortunately, we can bypass the problem with solid approximations. First, it is safe to claim that $\alpha_{i,1}$ is independent of $T_{i,1}$ and same for $\alpha_{i,2}$. This is because $\alpha_{i,1}$ is defined in

Eq. (5.7) and it only depends on the waiting time in the first entanglement swapping. Thus, we rewrite the postselection probability as

$$p_{i,ps} = \langle \alpha_{i,1} \rangle \langle \alpha_{i,2} \rangle \exp(-T_{i,dif} r). \tag{5.17}$$

Then, we substitute $T_{i,max}$ with $T_{i,min} + T_{i,dif}$, where $T_{i,min} = \min\{T_{i,1}, T_{i,2}\}$ and is independent with $T_{i,dif}$. If we define $\beta' = \langle T_{i,dif} p_{i,ps} \rangle / \langle T_{i,dif} \rangle \langle p_{i,ps} \rangle$, similar to Eq.5.12, we have

$$0 < \beta' < 1, \tag{5.18}$$

which gives the lower bound and upper bound of $T_{tot}^{(2)}$

$$\frac{\langle T_{min} \rangle}{\langle \alpha \rangle^2 \langle \exp(-T_{dif} r) \rangle} < \langle T_{tot}^{(2)} \rangle < \frac{\langle T_{max} \rangle}{\langle \alpha \rangle^2 \langle \exp(-T_{dif} r) \rangle}, \tag{5.19}$$

where we have used $\langle \alpha_{i,1} \rangle = \langle \alpha_{i,2} \rangle = \langle \alpha \rangle$ So far, we have not made assumptions on the probability distribution function on T_1 and T_2, which is necessary to derive the expectation value of T_{min}, T_{max}, and $\exp(-T_{dif} r)$. Here we assume the establishment time for one sublink, i.e., two elementary links, is mT_0, where the probability distribution function of m is $P(m)$ that defined in Eq. (5.1), except substituting p_0 for

$$p_0' = 2 p_0 \langle p_s \rangle / 3. \tag{5.20}$$

This assumption gives the same expectation value of establishment time for two links as given in Eq. (5.14), while the probability distribution function is different. In fact, the numerical evidence in Appendix B shows that substituting p_0 for p_0' in Eq. (5.2) and Eq. (5.3), gives a good approximation of the probability distribution function of T_{dif} and the expectation value of T_{min} and T_{max}. Thus, we can calculate the lower bound and the upper bound in Eq. (5.19), and similarly to the treatment in the two-photon BSM situation, we use the average of the lower bound and the upper bound to approximate $\langle T_{tot}^{(2)} \rangle$

$$\langle T_{tot}^{(2)} \rangle \approx \frac{\langle T_{max} \rangle + \langle T_{min} \rangle}{2 \langle \alpha \rangle^2 \langle \exp(-T_{dif} r) \rangle}. \tag{5.21}$$

5.1.2 Two-link repeater performance for different schemes

One can calculate the average entanglement distribution time from Eq. (5.21) and Eq. (5.15) for single-photon BSM and two-photon BSM. respectively. Here we give a detailed procedure of calculating repeater rates for each repeater scheme.

The "1 + 1" scheme. In the "1 + 1" scheme, the single photon emitted from each source will be partially transmitted to the central beam-splitter and the memory (controlled by a local beam-splitter). With one click after the central beam-splitter, i.e., the single-photon Bell-state measurement, the entanglement is claimed to be a success while a mixed state $\alpha^{(0)}|\Psi\rangle\langle\Psi|+(1-\alpha^{(0)})|0\rangle\langle 0|$ is produced. The success probability is $2\gamma(1-\gamma)\eta_t\eta_s\eta_d+2\gamma^2\eta_t(1-\eta_t)\eta_s\eta_d$, where γ is the transmission coefficient, $\eta_t=\exp(-L_0/L_{att})$ is the transmission loss, L_{att} the fiber attenuation length, and η_s is the single-photon source efficiency. The first term is the case that only one photon is sent to the central beam-splitter, while the second term represents both photons being sent to the central beam-splitter while one of the photons is lost due to the fiber attenuation. The success probability of entanglement generation can be approximated as

$$p_0 = 2\gamma\eta_t\eta_s\eta_d, \tag{5.22}$$

since $\eta_t \ll 1$. The fidelity of the resultant state with unity-efficiency quantum memory is $1-\gamma$, while an unsuccessful storage or retrieval of the photon will cause a vacuum component. Thus, considering memory efficiency η_m, the fidelity of the resultant state is

$$\alpha^{(0)} = \eta_m(1-\gamma). \tag{5.23}$$

It is important to note that the memory efficiency here is the product of the storage efficiency and the retrieval efficiency, i.e., the efficiency without considering decay.

Based on Eq. (5.7) and Eq. (5.8) and with $\alpha_1=\alpha^{(0)}$ and $\alpha_2=\alpha^{(0)}\exp(-n_{dif}^{(1)}r)$, we can derive the average fidelity after swapping

$$\langle\alpha^{(1)}\rangle = \langle\frac{\alpha^{(0)}\exp(-n_{dif}^{(1)}r)}{1+(1-\alpha^{(0)}\eta_d)\exp(-n_{dif}^{(1)}r)}\rangle, \tag{5.24}$$

and the average swapping probability

$$\langle p_s^{(1)} \rangle = \frac{\alpha^{(0)}\eta_d}{2}\langle 1 + (1-\alpha^{(0)}\eta_d)\exp(-n_{dif}^{(1)}r)\rangle. \tag{5.25}$$

The average entanglement distribution time can now be calculated via Eq. (5.21).

The "$\tilde{2}$ + 1" scheme. The "$\tilde{2}$ + 1" scheme is similar to the DLCZ scheme since the probability of photon-pair emission should be small to suppress multi-pair emission. It is important to recall that in Sec. 4.2 we do not distinguish the emission probability of non-deterministic photon source from the source efficiency of a deterministic photon source and call both the "source efficiency" η_s. The success probability of the state after entanglement generation can be easily derived as

$$p_0 = 2\eta_t\eta_s\eta_d \tag{5.26}$$

As $\eta_s \ll 1$, one can ignore the situation of coincident emission, and thus the fidelity of the resultant state is

$$\alpha^{(0)} = \eta_m. \tag{5.27}$$

Similarly, the average fidelity after swapping is

$$\langle \alpha^{(1)} \rangle = \langle \frac{\exp(-n_{dif}^{(1)}r)}{1+(1-\eta_d)\exp(-n_{dif}^{(1)}r)} \rangle, \tag{5.28}$$

and the average swapping probability is

$$\langle p_s^{(1)} \rangle = \frac{\eta_d}{2}\langle 1 + (1-\eta_d)\exp(-n_{dif}^{(1)}r)\rangle. \tag{5.29}$$

The "2 + 2" scheme and the "$\tilde{2}$ + 2" scheme. The calculation for the "2 + 2" scheme and the "$\tilde{2}$ + 2" scheme are the same, but it is worth noting that η_s for the non-deterministic source is much smaller than for the deterministic source. The probability generation probability for the "2 + 2" scheme and the "$\tilde{2}$ + 2" scheme is

$$p_0 = \eta_t^2\eta_s^2\eta_d^2/2, \tag{5.30}$$

where the one half is the intrinsic success probability of two-photon BSM. The fidelity of the created mixed state is

$$\alpha^{(0)} = \eta_m^2. \tag{5.31}$$

The average success probability can thus be derived from Eq. (5.10)

$$\langle p_s \rangle = \eta_d^2 \eta_m^4 \langle \exp(-n_{dif} r) \rangle / 2. \tag{5.32}$$

5.2 Implementation and limitations

In this section, we consider physical platforms for both quantum memories and photon sources. For quantum memories, we focus on rare-earth-ions(REIs) based memory [79–91] and Rydberg atom-ensemble (RA) memory [60, 92–95], which are evaluated in terms of memory lifetime and efficiency. As for photon sources, we consider quantum dots(QDs) as SPS [96, 97] and dPPS [98], Rydberg atoms as SPS [99, 100] and semi-dPPS [101], and spontaneous parametric down-conversion source as ndPPS [102, 103]. Thus, we propose the implementations for repeater schemes we mentioned in Sec. 4.2, shown in Tab. 5.1.

Table 5.1: Repeater scheme implementations (QDs: quantum dots; REIs: rare-earth-ions; RAs: Rydberg atoms; PDC: parametric-down conversion.)

Schemes	Implementations
$1+1$	QDs + REIs; RAs
$2+2$	QDs + REIs; RAs
$\tilde{2}+1$	PDC + REIs
$\tilde{2}+2$	PDC + REIs

5.2.1 Rare-earth-ions (REIs) based quantum memory

Rare-earth-ion doped crystals are attractive as quantum memories [104], with good performance in terms of storage efficiency [91, 105], multimode capacity [86, 106], and polarization qubit storage [107, 108]. At cryogenic temperatures, rare-earth-ion doped crystals exhibit long ground state coherence time: the electron spin coherence time of milliseconds is seen in many experiments [79, 80], and the nuclear spin coherence time can reach seconds or even hours [81–84].

The relevant transitions in rare-earth ions in solids have narrow homogeneous lines in combination with large inhomogeneous broadening. This can be used to create a periodic structure of narrow absorption peaks, a so-called atomic frequency comb (AFC) [37]. AFC is of great interest in the repeater applications since it allows efficient storage and readout of multiple temporal modes, which could greatly enhance the repeater performance [75]. The temporal modes ranging from dozens to thousands with a typical storage time of milliseconds level and efficiencies ranging from 1-35% [85–89]. Though theoretically the upper bound for the AFC quantum memory efficiency is unity, the requirement of a large optical depth [37] is hard to achieve. Putting the memory inside an asymmetric optical cavity can greatly enhance the efficiency by meeting the "impedance matching" condition [109]. So far, 53% [90] and 56% [91] memory efficiency have been reported in cavity-based AFC memory, with milliseconds storage time.

5.2.2 Rydberg atoms (RAs): Rydberg-state based photon sources and ground-state quantum memories

Rydberg states are characterized by a high principal quantum number and a corresponding large size [110]. Due to the large dipole moments and strong dipole-dipole interactions, the excitation of Rydberg atoms shifts the excited energy levels of nearby atoms, which excludes the resonant excitation of these atoms and is called the Rydberg-blockade [92]. The Rydberg-blockade, as the central topic of Rydberg atoms' application in quantum information processing, makes it possible to realize photon sources [99–101].

Both deterministic single-photon source (SPS) and semi-deterministic photon-pair source (PPS) can be realized in Rydberg atoms ensembles. The SPS relies on the Rydberg blockade effect, where the shifting in the energy level will inhibit transition into all but single-excitation states [92]. The spin-wave state is then converted into a light field by retrieving the excitation back to the intermediate level [99]. Room temperature SPS has also been demonstrated, though with low efficiency(4%) [100]. A semi-dPPS can also be realized via the Rydberg blockade effect, where two excitations with different momentum can be entangled. After mapping one excitation to a photon, a photon

and an atomic excitation can be entangled in the polarization domain. By further retrieving the ground-state excitation, the atom-photon entanglement is converted into a photon pair entanglement [101]. The intrinsic efficiency of this method is 50%, which is semi-deterministic. In the future, with more efficient qubit manipulation, 100% intrinsic efficiency, i.e., nPPS, can also be realized.

Cold atoms are also attractive as quantum memories since they allow both rapid and deterministic preparation of quantum states and their efficient transfer into single-photon light fields [60, 92–95]. Although the optical lifetime of highly excited Rydberg atoms can reach several hundred microseconds [110], the optical coherence time is only several microseconds [94] because Rydberg atoms are vary sensitive to the environment. Thus, to realize a long memory lifetime, we need to transfer the Rydberg excitation to a long-lived ground state. The demonstrated mapping efficiency from the Rydberg state to the ground state is already more than 70% [95]. The coherence time of the excitation stored in the ground state, is mainly limited by the motion of the atoms and the fluctuation of the residual magnetic field. Combining optical lattice, "clock state" storage and cavity enhancement read-out, 220ms spin-wave lifetime, and initial intrinsic retrieval efficiency of 76% have been demonstrated [60]. It is worth noting that the size of the Rydberg blockade radius poses a limitation on the number of atoms that can be used. The low optical depth will decrease the coupling strength between the single-photon and the ensemble, and thus the retrieval efficiency. It is therefore necessary to couple the ensemble with a cavity to enhance the overall efficiency.

5.2.3 Quantum dots (QDs) based single-photon and photon-pair source

Quantum dots(QDs) [111] are recognized as one of the best on-demand single-photon sources that possess the highest quantum efficiency in solid-state quantum emitter schemes [96]. In one experiment, near-perfect single-photon purity (99.1%), indistinguishability (98.6%), and high extraction efficiency (66%) have been reported based on resonant excitation of InAs-GaAs QDs in a micropillar cavity [97].

Photon-pair sources can also be realized by radiative cascades in quantum dots. In a recent

experiment, high fidelity (90%), pair extraction efficiency (62%), and indistinguishability (90%) are demonstrated by a single InGaAs quantum dot coupled to a circular Bragg grating bullseye cavity with broadband high Purcell factor up to 11.3 [98].

It is important to notice that the overall efficiency is usually limited by the scattering loss and fiber coupling efficiency, and the best overall efficiency is about 25% [112]. Fortunately, the photonic nanowire approach to fabricating efficient quantum light sources has been proposed [113] and shown great promise to achieve high extraction efficiency and high fiber coupling efficiency. The collective efficiency has realized 72% in single-photon source based on InAs QDs embedded in a GaAs photonic nanowire [114]. A photon-pair source has also been reported in nanowire quantum dots [115–117] with extraction efficiency around 15%. With further optimization of the nanowire shape, extraction efficiency of more than 90% can be expected [113].

5.2.4 Parametric down-conversion (PDC) based photon-pair source

One of the most widely-used techniques to produce entangled photon-pair is by spontaneous non-linear parametric processes. The process where one photon in the pumping laser goes through materials with second-order ($\chi^{(2)}$) nonlinearity and is converted into two photons is called spontaneous parametric down-conversion (SPDC). A similar process for third-order ($\chi^{(3)}$) materials is called spontaneous four-wave mixing(SFWM) [102]. Photons can be entangled in polarization, frequency, and time. A recent outstanding polarization-entanglement source uses narrow-band spectral filters that eliminate spectral correlations and has demonstrated high indistinguishability (97%) and purity (99%) [103]. It is important to note that, in order to suppress the multi-pair emission, the emission probability should be low and thus the photon-pair generation process is non-deterministic. On the other hand, it is relatively easy for this type of source to match the emission frequencies of each photon to a desired wavelength. For example, one photon can be in resonance with a quantum memory, while the other one matches the telecom band of optical fibers.

5.3 Numerical results

5.3.1 Memory requirements

We first study the repeater rates as a function of memory lifetime and efficiency. It is worth noting that the efficiency of photon sources should be predetermined to use Eq. (5.19) and Eq. (5.15) to calculate the repeater rates, defined as the reciprocal of EDT. We consider high, but realistic efficiencies of 75% and 50% for SPS and PPS, respectively, and the photon-pair emission probability 3% for ndPPS. The transmission coefficient $\gamma = 0.2$ in the "1 + 1" scheme, the fiber attenuation length $L_{att} = 22$km (for telecom-wavelength range around 1550nm), and the detector efficiency $\eta_d = 0.95$. In Fig. 5.1 we show the repeater rates for a total distance of 100 km, where the contour line represents the same repeater rates for various parameters of memory lifetime and efficiency.

The figures can provide useful information. To begin with, the graphs show the potential trade-off between memory lifetime and efficiency to achieve a target repeater rate, say 1 Hz. For example, in the "2 + 2" scheme, to realize the target repeater rate, one can use memories with 1ms lifetime and 50% efficiency, or with unity efficiency and 0.2ms lifetime, or with 15% efficiency and 1s lifetime.

One can find the most efficient way to improve the repeater performance by improving the memory parameter along the gradient in the contour graphs. In particular, one can see that for a short lifetime but high efficiency, there is limited benefit in improving the efficiency further and vice versa. Conversely, in the high lifetime regime (e.g. $>$ 10 ms for the "2 + 2" scheme), the gradients of the contour lines are parallel to the efficiency axis, meaning that the increase in efficiency will considerably improve the repeater rates. We also notice that the contour line is more concentrated in the small memory lifetime($<$ 1ms) and efficiency($<$ 20%) regime, which means an improvement in lifetime or efficiency respectively in the corresponding regimes will dramatically improve the repeater rates.

Moreover, the graphs give the upper bound of the repeater rates that can be achieved in these

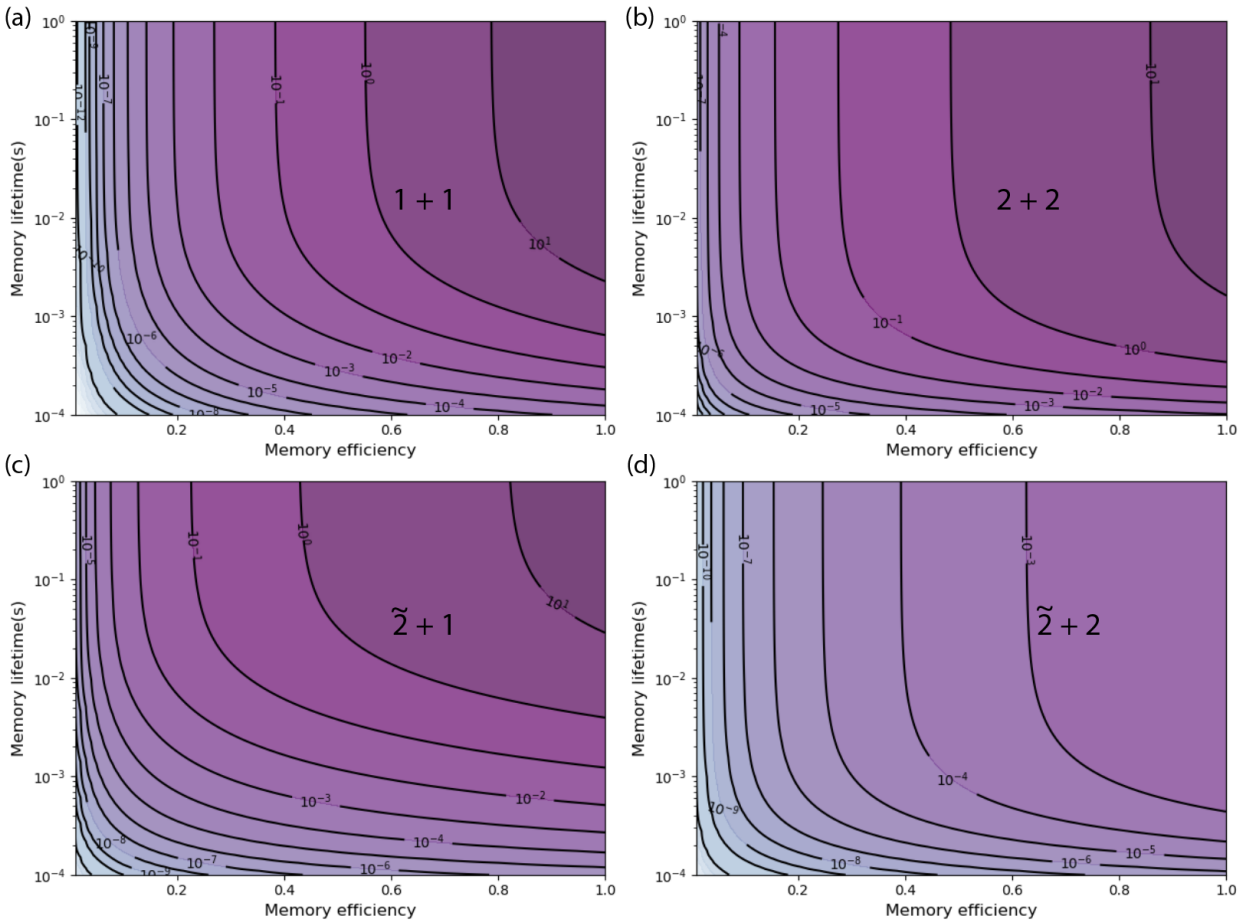

Figure 5.1: (Color online) Rates of various repeater schemes for a total distance of 100km. The numbers in the contour line represent the corresponding repeater rates in Hz. The plot shows the situation of two links(nesting level is 1). The corresponding repeater protocols and parameter regimes are (a) SPS + single-photon BSM($1+1$) with local beam-splitter transmission probability 0.8 and single-photon emission probability 0.75; (b)dPPS + two-photon BSM($2+2$) with photon–pair emission probability 0.5; (c)ndPPS + single-photon BSM($\tilde{2}+1$) with photon-pair emission probability 0.03; (d) ndPPS + two-photon BSM($\tilde{2}+2$) with photon-pair emission probability 0.03.

Table 5.2: Parameters for numerical calculation (QDs: quantum dots; REIs: rare-earth-ions; RAs: Rydberg atoms; PDC: parametric-down conversion; η_s: photon source efficiency; η_m quantum memory efficiency; τ_m quantum memory lifetime.)

Schemes	Implementations	Parameters
$1+1$	QDs + REIs	$\eta_s = 0.75$, $\eta_m = 0.7$, $\tau_m = 1$ms
	RAs	$\eta_s = 0.15$, $\eta_m = 0.75$, $\tau_m = 0.22$s
$2+2$	QDs + REIs	$\eta_s = 0.5$, $\eta_m = 0.7$, $\tau_m = 1$ms
	RAs	$\eta_s = 0.15$, $\eta_m = 0.75$, $\tilde{2}+2$
$\tilde{2}+1$ $\tilde{2}+2$	PDC + REIs	$\eta_s = 0.03$, $\eta_m = 0.7$, $\tau_m = 1$ms

schemes for this distance. The maximum repeater rate under the present assumptions is of order 10 Hz in the "1 + 1", "2 + 2", and "$\tilde{2}+1$" scheme and 10^{-3} Hz in the "$\tilde{2}+2$" scheme. These upper bounds of the repeater rates, which correspond to perfect quantum memories, can be improved by using better sources, more links, or multiplexing [16].

These results were obtained for exponential decay of memory efficiency as described in section III. In Appendix C we compare our results to what one would obtain under the common simplified assumption of a memory cut-off time. The main conclusion is that the cut-off is not a good approximation for short lifetimes.

5.3.2 Comparison of implementations

Let us now consider the practical implementations in Tab. 5.1, and give the expected repeater rates with realistic parameter regimes, shown in Tab. 5.2.

We plot the corresponding two-link repeater performance with various platforms as a function of distance in Fig. 5.2. The solid lines represent the performance of different implementations that are labeled on the figure. The schemes with more deterministic sources achieve higher rates, but even the schemes with non-deterministic sources can allow meaningful proof-of-principle demonstrations, especially the "$\tilde{2}$ + 1" scheme. Note that the rate for the "1 + 1" scheme with RAs decreases more slowly with distance under our assumptions compared with other implementations

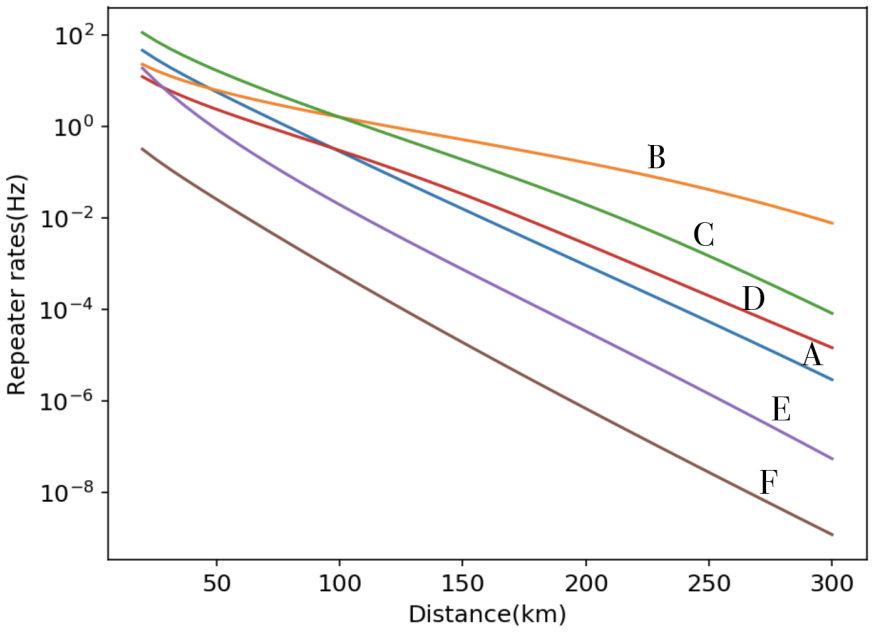

Figure 5.2: Comparison of repeater implementations with two links: the "1 + 1" scheme with QDs and REIs (A); the "1 + 1" scheme with RAs (B); the "2 + 2" scheme with QDs and REIs (C); the "2 + 2" scheme with RAs (D); the "$\tilde{2}$ + 1" scheme with PDC and REIs (E); the "$\tilde{2}$ + 2" scheme with PDC and REIs (F). (QDs: quantum dots; REIs: rare-earth-ions; RAs: Rydberg atoms; PDC: parametric-down conversion.)

mainly because of the longer memory lifetime.

It is possible to improve the repeater rates by adopting the optimized memory buffer time protocol of Ref. [118] that limits the entanglement generation time in elementary links. We discuss this approach in detail in Appendix D. The improvement is not dramatic in the considered regime for the two-link situation (first nesting level), but it might be more helpful for higher nesting levels.

Chapter 6

Conclusion and outlook

In this thesis, we studied quantum repeaters with both single-emitter based and ensemble-based quantum memories, and in particular, we considered imperfections of photon sources and quantum memories in a near-term situation with two repeater links and performed an analytical and numerical analysis of the latter. Our results provide guidance for the near-term implementation of long-distance quantum repeater demonstrations, suggesting that such demonstrations are within reach of current technology.

In our analysis, we have considered imperfections such as fiber photon loss, photon detector inefficiency, photon source inefficiency (for deterministic photon sources), quantum memory inefficiency, and finite lifetime. However, in realistic situations, other imperfections like multi-photon (pair) emission, non-identical photon sources and quantum memories, and phase instability cannot be ignored.

Note that the purpose of the calculations is not to beat direct transmission, but to give theoretical predictions for the natural next-step, i.e., realizing a two-link quantum repeater over a meaningful distance that demonstrates the entanglement swapping process between physical memories. Such demonstrations would be of significant importance since quantum repeaters with more links can be done in a similar manner.

To realize global quantum networks, we provide several comments for future studies. Firstly, the performance of quantum repeater links with minimal resources (considered in this thesis) has a limited range of distance that could provide a meaningful advantage over direct transmission. For example, the "1 + 1" scheme outperforms direct transmission for a distance of 580 km, with an entanglement generation time of 44 s, and this is even under the infinite-memory-lifetime assumption [16]. One could consider using schemes with multiplexing in frequency, time, or space to improve

the repeater rates, and this may require quantum memories and photon sources to have the corresponding feature. Besides, error-correction assisted quantum repeater protocols could also reduce the requirements on the quantum devices. Secondly, as we have mentioned the imperfections in implementing quantum repeaters come from many aspects: photon sources, memories, optical fibers, photon detectors, and etc. Improvements in all of these aspects are not possible to achieve for a single research team. One should recognize the importance of collaboration that could gather all these components with state-of-the-art development. Thirdly, different platforms are being investigated and no one could claim at this stage which is the best. Therefore, future quantum networks may consist of nodes with different implementations of photon sources and quantum memories. It is thus important to enable network nodes with different implementations to talk with each other. As different implementations may have distinct optical frequencies, quantum transductions would be necessary [119]. This may also require a uniform standard or agreement on both the hardware and software side to connect the quantum networks between different countries.

Appendix A

Detailed derivation of Eq. (5.14) and Eq. (5.15)

In this section, we give a detailed derivation of Eq. (5.14) and Eq. (5.15). Let us recall the original expression of EDT in Eq. (5.11), if we substitute $n_{r,max} = n_{r,min} + n_{r,dif}$, we will get

$$\begin{aligned} &(\sum_{r=1}^{k} n_{r,min} T_0) p_{k,s} \prod_{r=1}^{k-1} (1 - p_{r,s}) \\ +&(\sum_{r=1}^{k} n_{r,dif} T_0) p_{k,s} \prod_{r=1}^{k-1} (1 - p_{r,s}). \end{aligned} \tag{A.1}$$

To calculate the expectation time, we should average k, $n_{r,max}$, and $n_{r,dif}$(contained in p_s). The calculation for the first term in Eq. (A.1) is easy since p_s and n_{min} are independent, while it is hard in the second term where p_s depends on n_{dif}. Let us first give the expectation value of the first term. As $n_{r,dif}$ is independent of $p_{r,s}$, we derive

$$\begin{aligned} &T_0 \sum_{k=1}^{\infty} [(\sum_{r=1}^{k} \langle n_{r,min} \rangle) \langle p_{k,s} \rangle \prod_{r'=1}^{k-1} (1 - \langle p_{r',s} \rangle) \\ =&T_0 \sum_{k=1}^{\infty} [k \langle n_{r,min} \rangle \langle p_{k,s} \rangle \prod_{r'=1}^{k-1} (1 - \langle p_{r',s} \rangle)] \\ =&\frac{\langle n_{min} \rangle}{\langle p_s \rangle} T_0, \end{aligned} \tag{A.2}$$

where we have used the fact that the expectation of n_{min} and p_s are the same for different swapping attempts, i.e., $\langle n_{r,min} \rangle = \langle n_{min} \rangle$ and $\langle p_{r,s} \rangle = \langle p_s \rangle$.

To calculate the expectation value for the second term in Eq. (A.1), we need an assumption on the expectation value of $n_{r,dif} p_{r,s}$. As in the main text, we have defined $\beta = \langle n_{dif} p_s \rangle / \langle n_{dif} p_s \rangle$, where $0 < \beta < 1$. In the upper bound $\beta = 1$, the expectation value of the second term in Eq. (A.1)

can be expressed as

$$
\begin{aligned}
& T_0 \sum_{k=1}^{\infty} [(\sum_{r=1}^{k} \langle n_{r,dif} \rangle) \langle p_{k,s} \rangle \prod_{r'=1}^{k-1} (1 - \langle p_{r',s} \rangle) \\
=& T_0 \sum_{k=1}^{\infty} [k \langle n_{r,dif} \rangle \langle p_{k,s} \rangle \prod_{r'=1}^{k-1} (1 - \langle p_{r',s} \rangle)] \\
=& \frac{\langle n_{dif} \rangle}{\langle p_s \rangle} T_0,
\end{aligned}
\tag{A.3}
$$

while in the lower bound $\beta = 0$, the expectation value of the second term in Eq. (A.1) is negligible compared to the first term. Thus, depending on β, the average EDT is different. If $\beta = 1$, the average EDT is the sum of Eq. (A.2) and Eq. (A.3)

$$
\frac{\langle n_{min} \rangle}{\langle p_s \rangle} T_0 + \frac{\langle n_{dif} \rangle}{\langle p_s \rangle} T_0 = \frac{\langle n_{max} \rangle}{\langle p_s \rangle} T_0. \tag{A.4}
$$

On the other hand, if $\beta = 0$, the average EDT is simply the value in Eq. (A.2)

$$
\frac{\langle n_{min} \rangle}{\langle p_s \rangle} T_0. \tag{A.5}
$$

Appendix B

Numerical evidence for assumptions

In this section, we give the numerical evidence that supports our assumptions in the main text, especially Eq. (5.13) and Eq. (5.20). The parameter regime, if not specified, is $p_0 = 0.01$, $r = T_0/\tau_m = 1$, $\eta_d = 0.95$, and $\alpha^{(0)} = 1$.

First, let us give the numerical evidence for Eq. (5.13), i.e., $\beta = \langle n_{dif} * p_s \rangle / \langle n_{dif} \rangle \langle p_s \rangle \approx 1$ in single-photon BSM. We plot β as a function of p_0, shown in Fig. B.1(a-c) with different choices of state fidelity(after entanglement generation) and different lifetime regime. The result shows that the minimum ratio varies with different $p_0 - t_M$ regime and the lowest ratio in our considered regime is 84%, which means in Eq. (5.13), $\beta \approx 1$ is a good approximation. We also plot the ratio in the two-photon BSM scenario: in the low-p_0 regime, β is almost 0, while in the high-p_0 and high memory lifetime regime, β is close to 1. The ratio values 0 and 1 corresponds to the lower bound and upper bound in Eq. (5.15), respectively, and thus we approximate the average EDT using the average of lower bound and upper bound.

Secondly, we show the assumption in Eq. (5.20) is valid in the approximation of probability distribution of T_{dif} and the expectation value of T_{min} and T_{max}. Based on the probability assumption, we plot the theoretical predicted probability distribution of T_{dif} in comparison to the numerical result, shown in Fig. B.2. The four subfigures correspond to different $p_0 - t_M$ regimes and the theoretical results(red solid line) fit well with the numerical result(blue dots) in all considered parameter regimes. We also compare the theoretical and numerical results of the expectation value of T_{min} and T_{max}, shown in Fig. B.3. The theoretical results(blue dots) fit well with the numerical results (yellow crosses) for different τ_m (subfigures a and c) and p_0(subfigures b and d).

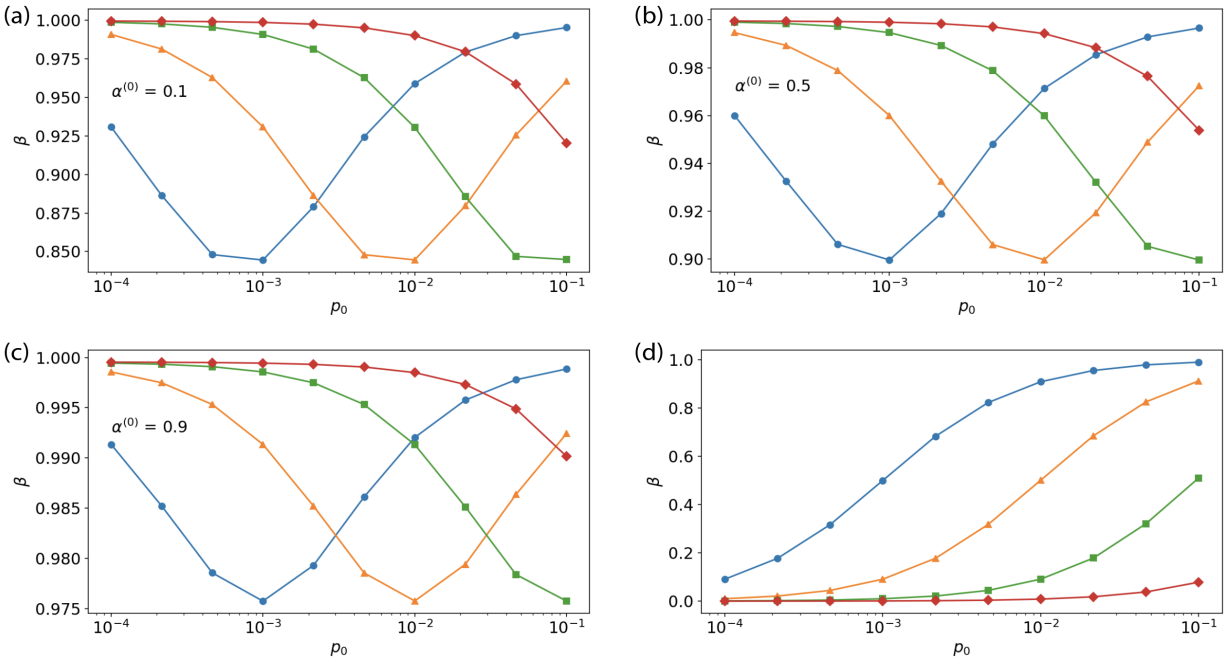

Figure B.1: (Color online) The relation between β and p_0 in different T_0/τ_m regime: $T_0/\tau_m = 0.001$(blue dots), 0.01(yellow triangles, 0.1(green squares), and 1(red diamonds). The first three subfigures shows results for single-photon BSM(a, b and c) and two-photon BSM(d). For single-photon BSM situation, we consider fidelity of the generated entangled state $\alpha^{(0)}$, which depends on the memory efficiency, as 0.9(a), 0.5(b) and 0.1(c).

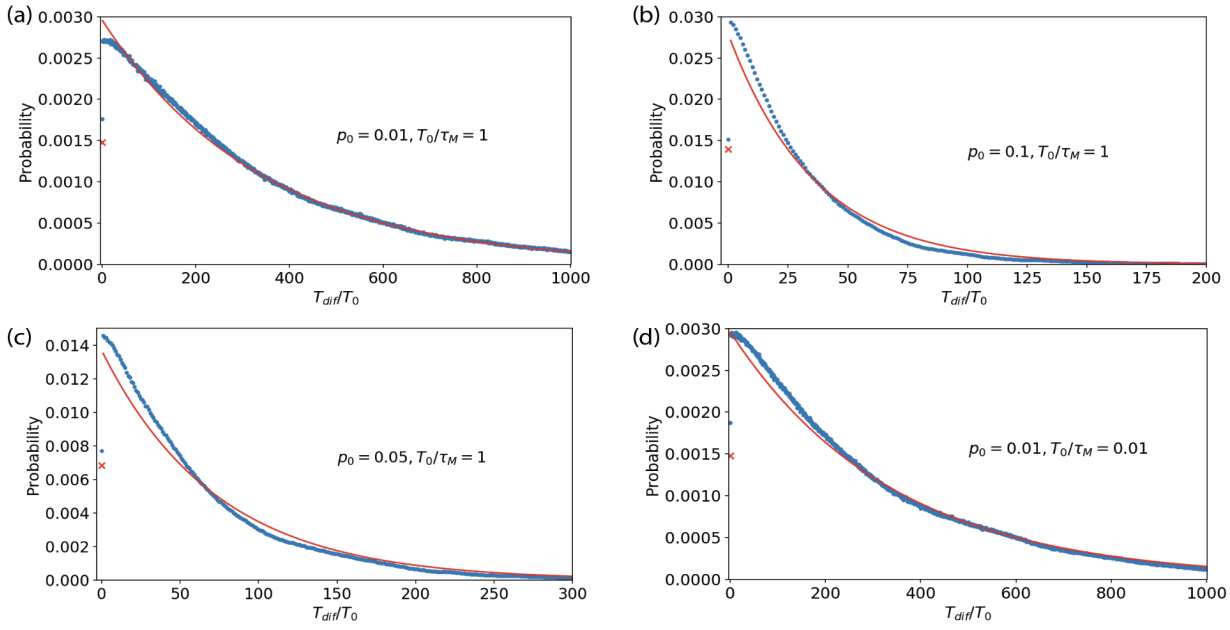

Figure B.2: (Color online) The numerical (blue dot) and theoretical (red solid line) probability distribution for T_{dif}. In the high-memory-lifetime regime ($T_0/\tau_m = 0.01$), low-memory-lifetime regime ($T_0/\tau_m = 1$), high-p_0 regime ($p_0 = 0.1$), and low-p_0 regime ($p_0 = 0.01$). The theoretical prediction fits well with the numerical result.

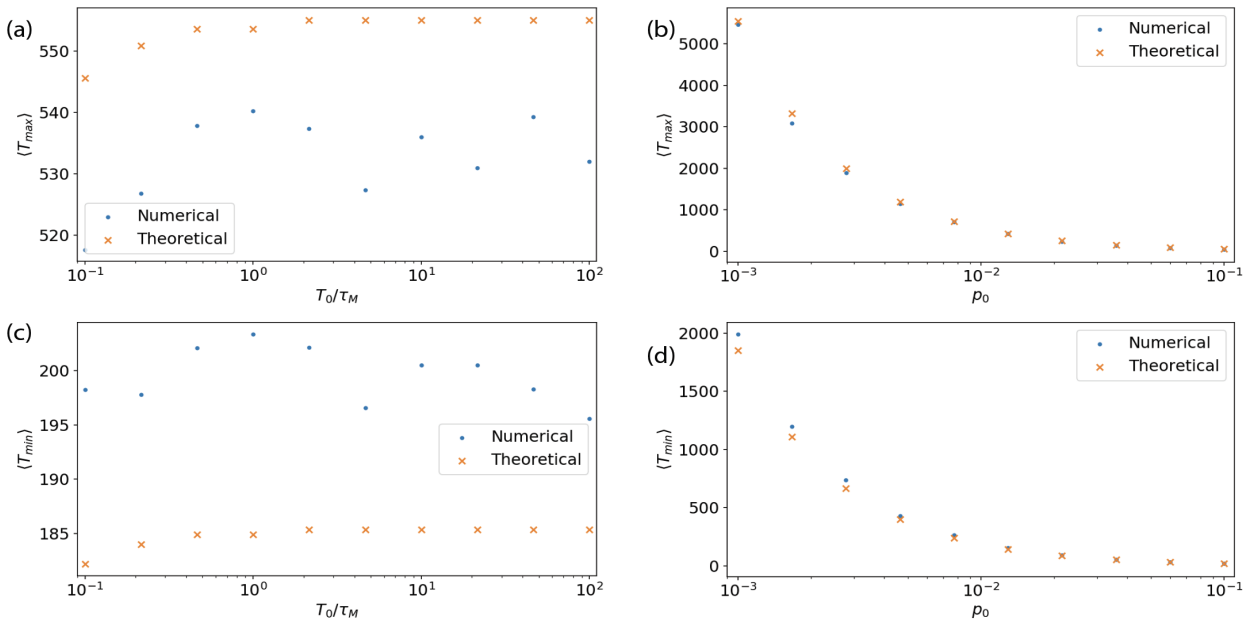

Figure B.3: (Color online) The numerical (blue dots) and theoretical (yellow xs) expectation value of T_{min} (a and b) and T_{max} (c and d). We plot the dependence on T_0/τ_m (a and c) and p_0 (c and d), and find the numerical results and theoretical results fit well.

Appendix C

Comparison of exponential decay and memory cut-off

In this section, we calculate the repeater rates using the memory cut-off assumption, and compare it with our result. Here we focus on the "2 + 2" scheme.

Given the initial memory state as $\alpha |\Psi\rangle \langle\Psi| + (1-\alpha)\rho$, the memory cut-off assumption is that after time t, the memory state is

$$F = \begin{cases} \alpha |\Psi\rangle \langle\Psi| + (1-\alpha)\rho & t \leq \tau \\ \rho' & t > \tau \end{cases}, \tag{C.1}$$

where ρ and ρ' are "unwanted states", and τ is usually the lifetime. It is clear that the fidelity and storage time are negatively correlated, and thus the lower bound and upper bound of the average EDT have the same expression as in Eq. (5.15). We notice the only difference is the average swapping probability $\langle p_s \rangle$. Without loss of generality, we assume the prefactor in Eq. (5.10) as 1, and therefore

$$p_s = \begin{cases} 1 & t \leq \tau_m/2 \\ 0 & t > \tau_m/2 \end{cases}, \tag{C.2}$$

where the $\tau_m/2$ is because in the "2 + 2" scheme, both memory will decay. Given $t = n_{dif} T_0$, and the probability distribution function as shown in Eq. (5.2), the expectation value of p_s is

$$\langle p_s \rangle_{cut} = 1 - \frac{2(1-p_0)^{\tau_m/2T_0}}{2-p_0}. \tag{C.3}$$

In comparison, with exponential memory decay, the swapping probability is shown in Eq. (5.32), and the expectation value is

$$\langle p_s \rangle_{exp} = \frac{p_0}{2-p_0} \frac{e^{T_0/\tau_m} + 1 - p_0}{e^{T_0/\tau_m} - 1 + p_0}. \tag{C.4}$$

We plot the average swapping probability under memory cut-off and exponential decay in different p_0 and τ_m/T_0 regimes, shown in Fig. C.1. In the high τ_m/T_0 regimes(>10), the memory

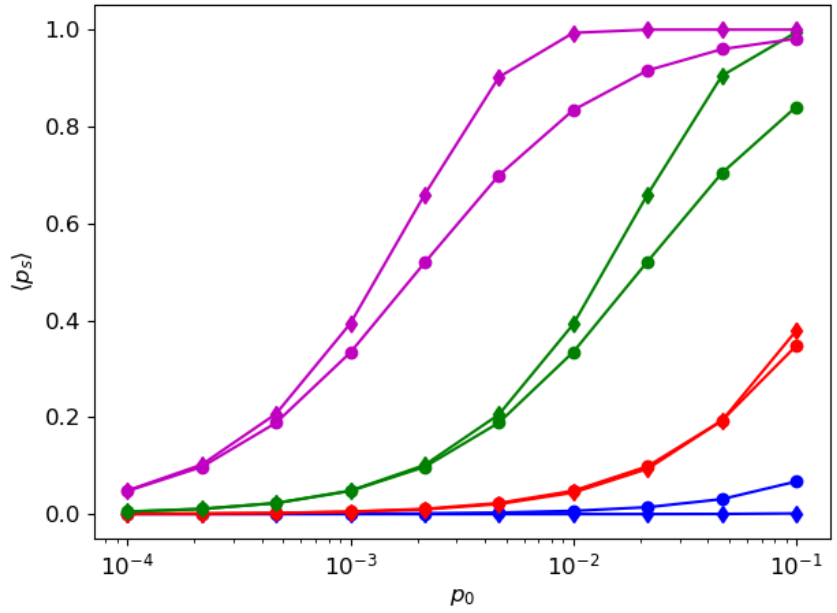

Figure C.1: (Color online) Average swapping probability in memory cut-off assumption $\langle p_s \rangle_{cut}$(diamond) and exponential decay assumption $\langle p_s \rangle_{exp}$(circle). The plots show the dependence of average swapping probability with different τ_m/T_0 regime: $\tau_m/T_0 = 1$(blue), 10(red), 100(green), and 1000(magenta).

cut-off seems to be a good assumption since the the two expectation values are well matched. However, in the low τ_m/T_0 regime($\ll$10), we find a distinct difference between the two value. For example, in the regime $\tau_m/T_0 = 1$, which is represented by blue lines in Fig. C.1, $\langle p_s \rangle_{cut}/\langle p_s \rangle_{exp} =$ 48.5 and 521 corresponding to $p_0 = 0.1$ and 0.01. Thus, in low memory time regime($\tau_m \sim T_0$), the memory cut-off is not a good approximation.

Appendix D

Improving the repeater rates with optimized memory buffer time

In this section, we focus on the two-photon BSM schemes ($2+2$ and $\tilde{2}+2$ scheme) with one nesting level. We consider the protocol of Ref. [118] where we abort the trial and start over again if the entanglement generation time of the elementary link exceeds a time threshold τ. Similarly to Eq. (5.11), the entanglement distribution time in this case is thus

$$T(\tau) = \sum_{k=1}^{\infty} [(\sum_{r=1}^{k} \min\{n_{r,max} T_0, \tau\}) p'_{k,s} \prod_{r=1}^{k-1} (1 - p'_{r,s})]. \tag{D.1}$$

Here $p'_{r,s}$ is the swapping probability in the rth swapping attempt, and depends on τ as

$$p'_{r,s} = \begin{cases} p_s & n_{max} \leq \tau / T_0 \\ 0 & n_{max} > \tau / T_0 \end{cases} \tag{D.2}$$

which is independent of r. Here p_s is the swapping probability defined in Eq. (5.32) and is a function of n_{dif}. For simplicity, we calculate the upper bound of the expectation value of $T(\tau)$

$$\langle T(\tau) \rangle \approx \frac{\langle \min\{n_{max} T_0, \tau\} \rangle}{\langle p'_s \rangle}, \tag{D.3}$$

where we have used the condition that $\langle n_{r,max} \rangle = \langle n_{max} \rangle$ and $\langle p'_{r,s} \rangle = \langle p'_s \rangle$ for all r. The numerator in Eq. (D.3) can be calculated with the PDF for n_{max}, which is defined as

$$P(n_{max}) = 2 \sum_{i=1}^{n_{max}-1} P(i, n_{max}) + P(n_{max}, n_{max}), \tag{D.4}$$

where $P(n_1, n_2) = p_0^2 (1 - p_0)^{n_1 + n_2 - 2}$ is the joint PDF of n_1 and n_2 defined in Sec. 5.1.1. Thus,

$$\begin{aligned} &\langle \min\{n'_{max} T_0, \tau\} \rangle \\ &= \sum_{n_{max}=1}^{\tau/T_0} n_{max} T_0 P(n_{max}) + \sum_{n_{max}=\tau/T_0+1}^{\infty} \tau P(n_{max}). \end{aligned} \tag{D.5}$$

Calculating the denominator requires the conditional probability (conditioned on $n_{max} \leq \tau/T_0$) of n_{dif}. The joint probability of n_{dif} and n_{max} is

$$P(n_{dif}, n_{max}) = 2P(n_1 = n_{max}, n_2 = n_{max} - n_{dif}). \tag{D.6}$$

The conditional probability is

$$\begin{aligned} P_c(n_{dif}) &= P(n_{dif} | n_{max} \leq \tau/T_0) \\ &= \frac{\sum_{n_{max}=n_{dif}+1}^{\tau/T_0} P(n_{dif}, n_{max})}{\sum_{n_{max}=n_{dif}+1}^{\tau/T_0} P(n_{max})}. \end{aligned} \tag{D.7}$$

We can now calculate the denominator as

$$\langle p_s' \rangle = \sum_{n_{dif}=0}^{\tau/T_0-1} p_s(n_{dif}) P_c(n_{dif}). \tag{D.8}$$

Now the average entanglement distribution time defined in Eq. (D.3) can be calculated with Eq. (D.5) and Eq. (D.7). Considering τ_0 such that $\langle T(\tau_0) \rangle = \max \langle T(\tau) \rangle$, we define

$$\lambda = \frac{\langle T(\infty) \rangle}{\langle T(\tau_0) \rangle}, \tag{D.9}$$

representing the ratio of entanglement distribution rates for the case with and without limited memory buffer time.

In the numerical calculation, we use detector efficiency $\eta_d = 0.95$ and memory efficiency $\eta_m = 0.5$, and thus λ only depends on the memory lifetime τ_m and the entanglement generation probability p_0. To give an example, we plot the dependence of the average entanglement distribution time on the time threshold τ in the case that $p_0 = 0.1$, and $\tau_m = 10T_0$, see Fig. D.1. As the time threshold increases, the average entanglement generation time first decreases and reaches a minimum value at τ_0. Then it increases and finally reaches $\langle T(\infty) \rangle$.

To see how the ratio λ depends on p_0 and τ_m, we plot the numerical results in Fig. D.2. It is clear that the improvement of the repeater rates is concentrated in the low-τ_m, low-p_0 regime. The maximum ratio in the considered regime is about 2.4.

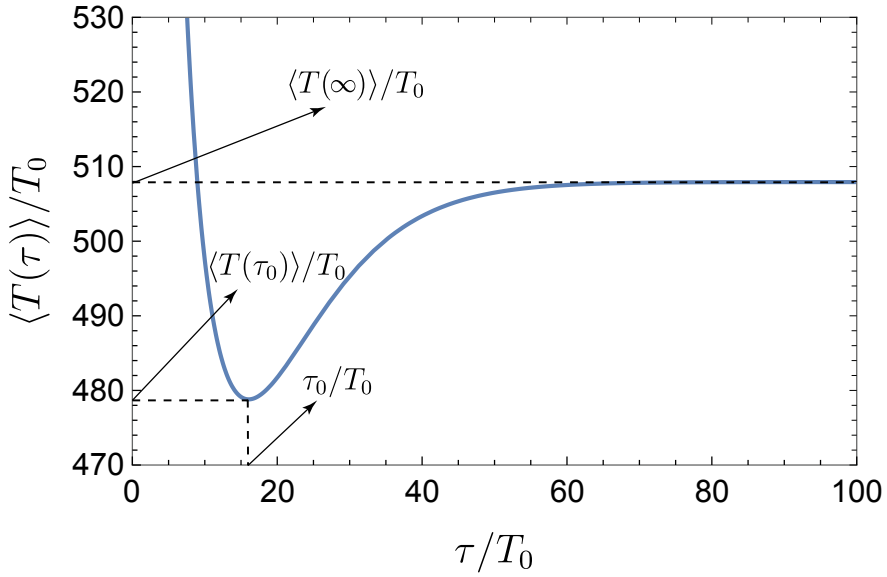

Figure D.1: Average entanglement distribution time with limited entanglement generation time. The parameters used are $\eta_d = 0.95$, $\eta_m = 0.5$, $p_0 = 0.1$, and $\tau_m = 10T_0$. The minimum value (maximum rate) is obtained with $\tau_0 \approx 16T_0$, and $\lambda \approx 1.06$.

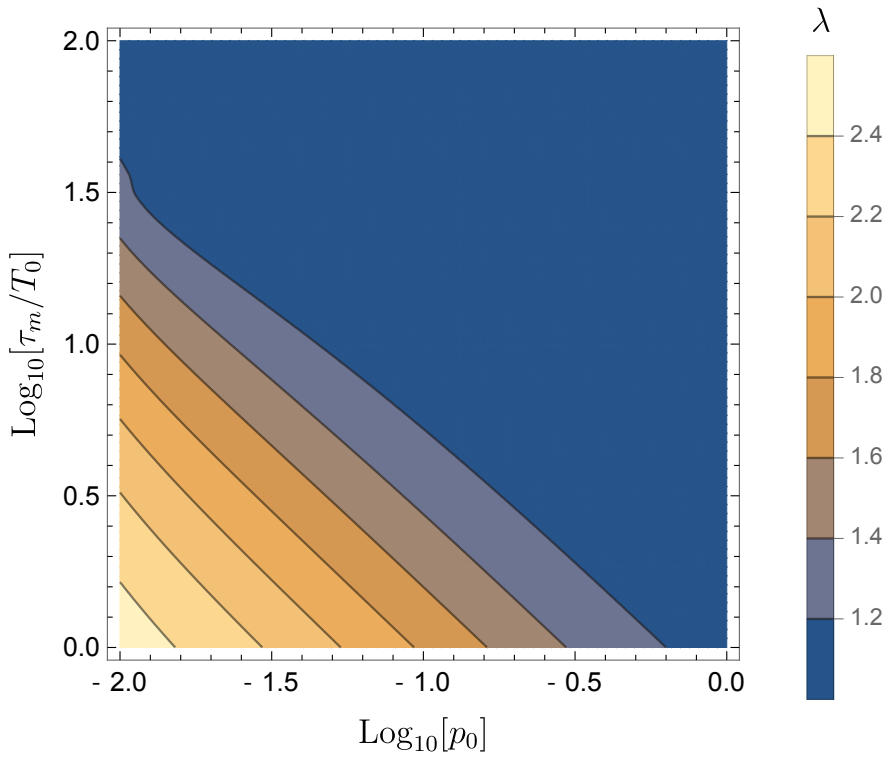

Figure D.2: (Color online) The ratio λ of Eq. (D9), which represents the improvement achieved by optimizing the memory buffer time.

Bibliography

[1] Michael A Nielsen and Isaac Chuang. Quantum computation and quantum information, 2002.

[2] Richard P Feynman. Simulating physics with computers. *Int. J. Theor. Phys*, 21(6/7), 1999.

[3] Peter W Shor. Polynomial-time algorithms for prime factorization and discrete logarithms on a quantum computer. *SIAM review*, 41(2):303–332, 1999.

[4] Lov K Grover. A fast quantum mechanical algorithm for database search. In *Proceedings of the twenty-eighth annual ACM symposium on Theory of computing*, pages 212–219, 1996.

[5] Frank Arute, Kunal Arya, Ryan Babbush, Dave Bacon, Joseph C Bardin, Rami Barends, Rupak Biswas, Sergio Boixo, Fernando GSL Brandao, David A Buell, et al. Quantum supremacy using a programmable superconducting processor. *Nature*, 574(7779):505–510, 2019.

[6] Stephen Wiesner. Conjugate coding. *SIGACT News*, 15(1):78–88, January 1983.

[7] Charles H Bennett and Gilles Brassard. Quantum cryptography: Public key distribution and coin tossing. *arXiv preprint arXiv:2003.06557*, 2020.

[8] Hoi-Kwong Lo and Hoi Fung Chau. Unconditional security of quantum key distribution over arbitrarily long distances. *science*, 283(5410):2050–2056, 1999.

[9] Daniel Gottesman, H-K Lo, Norbert Lutkenhaus, and John Preskill. Security of quantum key distribution with imperfect devices. In *International Symposium onInformation Theory, 2004. ISIT 2004. Proceedings.*, page 136. IEEE, 2004.

[10] Renato Renner. Security of quantum key distribution. *International Journal of Quantum Information*, 6(01):1–127, 2008.

[11] Ji-Gang Ren, Ping Xu, Hai-Lin Yong, Liang Zhang, Sheng-Kai Liao, Juan Yin, Wei-Yue Liu, Wen-Qi Cai, Meng Yang, Li Li, et al. Ground-to-satellite quantum teleportation. *Nature*, 549(7670):70, 2017.

[12] Sheng-Kai Liao, Wen-Qi Cai, Wei-Yue Liu, Liang Zhang, Yang Li, Ji-Gang Ren, Juan Yin, Qi Shen, Yuan Cao, Zheng-Ping Li, et al. Satellite-to-ground quantum key distribution. *Nature*, 549(7670):43–47, 2017.

[13] Alberto Boaron, Gianluca Boso, Davide Rusca, Cédric Vulliez, Claire Autebert, Misael Caloz, Matthieu Perrenoud, Gaëtan Gras, Félix Bussières, Ming-Jun Li, et al. Secure quantum key distribution over 421 km of optical fiber. *Physical review letters*, 121(19):190502, 2018.

[14] James L Park. The concept of transition in quantum mechanics. *Foundations of Physics*, 1(1):23–33, 1970.

[15] H-J Briegel, Wolfgang Dür, Juan I Cirac, and Peter Zoller. Quantum repeaters: the role of imperfect local operations in quantum communication. *Physical Review Letters*, 81(26):5932, 1998.

[16] Nicolas Sangouard, Christoph Simon, Hugues De Riedmatten, and Nicolas Gisin. Quantum repeaters based on atomic ensembles and linear optics. *Reviews of Modern Physics*, 83(1):33, 2011.

[17] H Jeff Kimble. The quantum internet. *Nature*, 453(7198):1023–1030, 2008.

[18] Christoph Simon. Towards a global quantum network. *Nature Photonics*, 11(11):678–680, 2017.

[19] Stephanie Wehner, David Elkouss, and Ronald Hanson. Quantum internet: A vision for the road ahead. *Science*, 362(6412):eaam9288, 2018.

[20] Hiroki Takesue, Sae Woo Nam, Qiang Zhang, Robert H Hadfield, Toshimori Honjo, Kiyoshi Tamaki, and Yoshihisa Yamamoto. Quantum key distribution over a 40-db channel loss using superconducting single-photon detectors. *Nature photonics*, 1(6):343, 2007.

[21] Hua-Lei Yin, Teng-Yun Chen, Zong-Wen Yu, Hui Liu, Li-Xing You, Yi-Heng Zhou, Si-Jing Chen, Yingqiu Mao, Ming-Qi Huang, Wei-Jun Zhang, et al. Measurement-device-independent quantum key distribution over a 404 km optical fiber. *Physical review letters*, 117(19):190501, 2016.

[22] Peter C Humphreys, Norbert Kalb, Jaco PJ Morits, Raymond N Schouten, Raymond FL Vermeulen, Daniel J Twitchen, Matthew Markham, and Ronald Hanson. Deterministic delivery of remote entanglement on a quantum network. *Nature*, 558(7709):268–273, 2018.

[23] Longest microwave quantum link. *ETHz News*, Mar 2020.

[24] Masahide Sasaki, M Fujiwara, H Ishizuka, W Klaus, K Wakui, M Takeoka, S Miki, T Yamashita, Z Wang, A Tanaka, et al. Field test of quantum key distribution in the tokyo qkd network. *Optics express*, 19(11):10387–10409, 2011.

[25] Paul Jouguet, Sébastien Kunz-Jacques, Thierry Debuisschert, Simon Fossier, Eleni Diamanti, Romain Alléaume, Rosa Tualle-Brouri, Philippe Grangier, Anthony Leverrier, Philippe Pache, et al. Field test of classical symmetric encryption with continuous variables quantum key distribution. *Optics Express*, 20(13):14030–14041, 2012.

[26] Shuang Wang, Wei Chen, Zhen-Qiang Yin, Hong-Wei Li, De-Yong He, Yu-Hu Li, Zheng Zhou, Xiao-Tian Song, Fang-Yi Li, Dong Wang, et al. Field and long-term demonstration of a wide area quantum key distribution network. *Optics express*, 22(18):21739–21756, 2014.

[27] Matthias Ulrich Staudt, Mikael Afzelius, Hugues De Riedmatten, Sara Rose Hastings-Simon, Christoph Simon, R Ricken, H Suche, W Sohler, and Nicolas Gisin. Interference

of multimode photon echoes generated in spatially separated solid-state atomic ensembles. *Physical review letters*, 99(17):173602, 2007.

[28] Stephen C Wein, Jia-Wei Ji, Yu-Feng Wu, Faezeh Kimiaee Asadi, Roohollah Ghobadi, and Christoph Simon. Analyzing photon-counting based entanglement generation between solid-state spin qubits by unraveling the master equation. *arXiv preprint arXiv:2004.04786*, 2020.

[29] Yufeng Wu, Jianlong Liu, and Christoph Simon. Near-term performance of quantum repeaters with imperfect ensemble-based quantum memories. *Physical Review A*, 101(4):042301, 2020.

[30] Yong Yu, Fei Ma, Xi-Yu Luo, Bo Jing, Peng-Fei Sun, Ren-Zhou Fang, Chao-Wei Yang, Hui Liu, Ming-Yang Zheng, Xiu-Ping Xie, et al. Entanglement of two quantum memories via fibres over dozens of kilometres. *Nature*, 578(7794):240–245, 2020.

[31] Jian-Wei Pan, Christoph Simon, Časlav Brukner, and Anton Zeilinger. Entanglement purification for quantum communication. *Nature*, 410(6832):1067–1070, 2001.

[32] Mete Atatüre, Dirk Englund, Nick Vamivakas, Sang-Yun Lee, and Joerg Wrachtrup. Material platforms for spin-based photonic quantum technologies. *Nature Reviews Materials*, 3(5):38–51, 2018.

[33] Ronald Hanson, Leo P Kouwenhoven, Jason R Petta, Seigo Tarucha, and Lieven MK Vandersypen. Spins in few-electron quantum dots. *Reviews of modern physics*, 79(4):1217, 2007.

[34] Vitaly N Golovach, Alexander Khaetskii, and Daniel Loss. Phonon-induced decay of the electron spin in quantum dots. *Physical review letters*, 93(1):016601, 2004.

[35] Liang Jiang, Jacob M Taylor, Kae Nemoto, William J Munro, Rodney Van Meter, and

Mikhail D Lukin. Quantum repeater with encoding. *Physical Review A*, 79(3):032325, 2009.

[36] L-M Duan, Mikhail D Lukin, J Ignacio Cirac, and Peter Zoller. Long-distance quantum communication with atomic ensembles and linear optics. *Nature*, 414(6862):413–418, 2001.

[37] Mikael Afzelius, Christoph Simon, Hugues de Riedmatten, and Nicolas Gisin. Multimode quantum memory based on atomic frequency combs. *Phys. Rev. A*, 79:052329, May 2009.

[38] S Bose, PL Knight, MB&amp Plenio, and V Vedral. Proposal for teleportation of an atomic state via cavity decay. *Physical Review Letters*, 83(24):5158, 1999.

[39] Carlos Cabrillo, J Ignacio Cirac, Pablo Garcia-Fernandez, and Peter Zoller. Creation of entangled states of distant atoms by interference. *Physical Review A*, 59(2):1025, 1999.

[40] Daniel E Browne, Martin B Plenio, and Susana F Huelga. Robust creation of entanglement between ions in spatially separate cavities. *Physical review letters*, 91(6):067901, 2003.

[41] Sean D Barrett and Pieter Kok. Efficient high-fidelity quantum computation using matter qubits and linear optics. *Physical Review A*, 71(6):060310, 2005.

[42] L Childress, JM Taylor, Anders Søndberg Sørensen, and Mikhail D Lukin. Fault-tolerant quantum repeaters with minimal physical resources and implementations based on single-photon emitters. *Physical Review A*, 72(5):052330, 2005.

[43] Lilian Childress, JM Taylor, Anders Søndberg Sørensen, and MD Lukin. Fault-tolerant quantum communication based on solid-state photon emitters. *Physical review letters*, 96(7):070504, 2006.

[44] F Kimiaee Asadi, N Lauk, S Wein, N Sinclair, C O'Brien, and C Simon. Quantum repeaters with individual rare-earth ions at telecommunication wavelengths. *Quantum*, 2:93, 2018.

[45] Filip Rozpedek, Raja Yehia, Kenneth Goodenough, Maximilian Ruf, Peter C Humphreys, Ronald Hanson, Stephanie Wehner, and David Elkouss. Near-term quantum-repeater experiments with nitrogen-vacancy centers: Overcoming the limitations of direct transmission. *Physical Review A*, 99(5):052330, 2019.

[46] Sourabh Kumar, Nikolai Lauk, and Christoph Simon. Towards long-distance quantum networks with superconducting processors and optical links. *Quantum Science and Technology*, 4(4):045003, 2019.

[47] Roohollah Ghobadi, Stephen Wein, Hamidreza Kaviani, Paul Barclay, and Christoph Simon. Progress toward cryogen-free spin-photon interfaces based on nitrogen-vacancy centers and optomechanics. *Physical Review A*, 99(5):053825, 2019.

[48] L Jiang, JM Taylor, and MD Lukin. Fast and robust approach to long-distance quantum communication with atomic ensembles. *Physical Review A*, 76(1):012301, 2007.

[49] DA Gangloff, Gabriel Éthier-Majcher, Constantin Lang, EV Denning, JH Bodey, DM Jackson, Edmund Clarke, Maxime Hugues, Claire Le Gall, and Mete Atatüre. Quantum interface of an electron and a nuclear ensemble. *Science*, 364(6435):62–66, 2019.

[50] Lilian Childress and Ronald Hanson. Diamond nv centers for quantum computing and quantum networks. *MRS bulletin*, 38(2):134–138, 2013.

[51] L Childress, MV Gurudev Dutt, JM Taylor, AS Zibrov, F Jelezko, J Wrachtrup, PR Hemmer, and MD Lukin. Coherent dynamics of coupled electron and nuclear spin qubits in diamond. *Science*, 314(5797):281–285, 2006.

[52] Julien Laurat, Hugues De Riedmatten, Daniel Felinto, Chin-Wen Chou, Erik W Schomburg, and H Jeff Kimble. Efficient retrieval of a single excitation stored in an atomic ensemble. *Optics express*, 14(15):6912–6918, 2006.

[53] Jonathan Simon, Haruka Tanji, Saikat Ghosh, and Vladan Vuletić. Single-photon bus connecting spin-wave quantum memories. *Nature Physics*, 3(11):765–769, 2007.

[54] A Kuzmich, WP Bowen, AD Boozer, A Boca, CW Chou, L-M Duan, and HJ Kimble. Generation of nonclassical photon pairs for scalable quantum communication with atomic ensembles. *Nature*, 423(6941):731–734, 2003.

[55] Caspar H van der Wal, Matthew D Eisaman, Axel André, Ronald L Walsworth, David F Phillips, Alexander S Zibrov, and Mikhail D Lukin. Atomic memory for correlated photon states. *Science*, 301(5630):196–200, 2003.

[56] DN Matsukevich and A Kuzmich. Quantum state transfer between matter and light. *Science*, 306(5696):663–666, 2004.

[57] Chin-Wen Chou, Hugues de Riedmatten, Daniel Felinto, Sergey V Polyakov, Steven J Van Enk, and H Jeff Kimble. Measurement-induced entanglement for excitation stored in remote atomic ensembles. *Nature*, 438(7069):828–832, 2005.

[58] Chin-Wen Chou, Julien Laurat, Hui Deng, Kyung Soo Choi, Hugues De Riedmatten, Daniel Felinto, and H Jeff Kimble. Functional quantum nodes for entanglement distribution over scalable quantum networks. *Science*, 316(5829):1316–1320, 2007.

[59] Zhen-Sheng Yuan, Yu-Ao Chen, Bo Zhao, Shuai Chen, Jörg Schmiedmayer, and Jian-Wei Pan. Experimental demonstration of a bdcz quantum repeater node. *Nature*, 454(7208):1098–1101, 2008.

[60] Sheng-Jun Yang, Xu-Jie Wang, Xiao-Hui Bao, and Jian-Wei Pan. An efficient quantum light–matter interface with sub-second lifetime. *Nature Photonics*, 10(6):381, 2016.

[61] YF Pu, N Jiang, W Chang, HX Yang, C Li, and LM Duan. Experimental realization of a multiplexed quantum memory with 225 individually accessible memory cells. *Nature communications*, 8:15359, 2017.

[62] CK Hong and L Mandel. Theory of parametric frequency down conversion of light. *Physical Review A*, 31(4):2409, 1985.

[63] MJ Collett and DF Walls. Quantum limits to light amplifiers. *Physical review letters*, 61(21):2442, 1988.

[64] Nicolas Sangouard, Christoph Simon, Jiří Minář, Hugo Zbinden, Hugues De Riedmatten, and Nicolas Gisin. Long-distance entanglement distribution with single-photon sources. *Physical Review A*, 76(5):050301, 2007.

[65] Christoph Simon, Hugues De Riedmatten, Mikael Afzelius, Nicolas Sangouard, Hugo Zbinden, and Nicolas Gisin. Quantum repeaters with photon pair sources and multimode memories. *Physical review letters*, 98(19):190503, 2007.

[66] Zeng-Bing Chen, Bo Zhao, Yu-Ao Chen, Jörg Schmiedmayer, and Jian-Wei Pan. Fault-tolerant quantum repeater with atomic ensembles and linear optics. *Physical Review A*, 76(2):022329, 2007.

[67] Bo Zhao, Zeng-Bing Chen, Yu-Ao Chen, Jörg Schmiedmayer, and Jian-Wei Pan. Robust creation of entanglement between remote memory qubits. *Physical review letters*, 98(24):240502, 2007.

[68] Neil Sinclair, Erhan Saglamyurek, Hassan Mallahzadeh, Joshua A Slater, Mathew George, Raimund Ricken, Morgan P Hedges, Daniel Oblak, Christoph Simon, Wolfgang Sohler, et al. Spectral multiplexing for scalable quantum photonics using an atomic frequency comb quantum memory and feed-forward control. *Physical review letters*, 113(5):053603, 2014.

[69] Hari Krovi, Saikat Guha, Zachary Dutton, Joshua A Slater, Christoph Simon, and Wolfgang Tittel. Practical quantum repeaters with parametric down-conversion sources. *Applied Physics B*, 122(3):52, 2016.

[70] Taehyun Kim, Marco Fiorentino, and Franco NC Wong. Phase-stable source of polarization-entangled photons using a polarization sagnac interferometer. *Physical Review A*, 73(1):012316, 2006.

[71] Xiao-Hui Bao, Xiao-Fan Xu, Che-Ming Li, Zhen-Sheng Yuan, Chao-Yang Lu, and Jian-Wei Pan. Quantum teleportation between remote atomic-ensemble quantum memories. *Proceedings of the National Academy of Sciences*, 109(50):20347–20351, 2012.

[72] Wolfgang Pfaff, Bas J Hensen, Hannes Bernien, Suzanne B van Dam, Machiel S Blok, Tim H Taminiau, Marijn J Tiggelman, Raymond N Schouten, Matthew Markham, Daniel J Twitchen, et al. Unconditional quantum teleportation between distant solid-state quantum bits. *Science*, 345(6196):532–535, 2014.

[73] G Vittorini, D Hucul, IV Inlek, C Crocker, and C Monroe. Entanglement of distinguishable quantum memories. *Physical Review A*, 90(4):040302, 2014.

[74] Jonatan Bohr Brask and Anders Søndberg Sørensen. Memory imperfections in atomic-ensemble-based quantum repeaters. *Physical Review A*, 78(1):012350, 2008.

[75] OA Collins, SD Jenkins, A Kuzmich, and TAB Kennedy. Multiplexed memory-insensitive quantum repeaters. *Physical review letters*, 98(6):060502, 2007.

[76] E Shchukin, F Schmidt, and P van Loock. Waiting time in quantum repeaters with probabilistic entanglement swapping. *Physical Review A*, 100(3):032322, 2019.

[77] Sumeet Khatri, Corey T Matyas, Aliza U Siddiqui, and Jonathan P Dowling. Practical figures of merit and thresholds for entanglement distribution in quantum networks. *Physical Review Research*, 1(2):023032, 2019.

[78] Carsten Schuck, Wolfram HP Pernice, and Hong X Tang. Waveguide integrated low noise nbtin nanowire single-photon detectors with milli-hz dark count rate. *Scientific reports*, 3:1893, 2013.

[79] P Siyushev, K Xia, R Reuter, M Jamali, N Zhao, N Yang, C Duan, N Kukharchyk, AD Wieck, R Kolesov, et al. Coherent properties of single rare-earth spin qubits. *Nature communications*, 5:3895, 2014.

[80] Kangwei Xia, Roman Kolesov, Ya Wang, Petr Siyushev, Rolf Reuter, Thomas Kornher, Nadezhda Kukharchyk, Andreas D Wieck, Bruno Villa, Sen Yang, et al. All-optical preparation of coherent dark states of a single rare earth ion spin in a crystal. *Physical review letters*, 115(9):093602, 2015.

[81] Elliott Fraval, MJ Sellars, and JJ Longdell. Dynamic decoherence control of a solid-state nuclear-quadrupole qubit. *Physical review letters*, 95(3):030506, 2005.

[82] Jevon J Longdell, Elliot Fraval, Matthew J Sellars, and Neil B Manson. Stopped light with storage times greater than one second using electromagnetically induced transparency in a solid. *Physical review letters*, 95(6):063601, 2005.

[83] Manjin Zhong, Morgan P. Hedges, Rose L. Ahlefeldt, John G. Bartholomew, Sarah E. Beavan, Sven M. Wittig, Jevon J. Longdell, and Matthew J. Sellars. Optically addressable nuclear spins in a solid with a six-hour coherence time. *Nature*, 517(7533):177–180, jan 2015.

[84] Miloš Rančić, Morgan P. Hedges, Rose L. Ahlefeldt, and Matthew J. Sellars. Coherence time of over a second in a telecom-compatible quantum memory storage material. *Nature Physics*, 14(1):50–54, sep 2017.

[85] Mahmood Sabooni, F Beaudoin, Andreas Walther, N Lin, Atia Amari, Maomao Huang, and Stefan Kröll. Storage and recall of weak coherent optical pulses with an efficiency of 25%. *Physical review letters*, 105(6):060501, 2010.

[86] Imam Usmani, Mikael Afzelius, Hugues De Riedmatten, and Nicolas Gisin. Mapping mul-

tiple photonic qubits into and out of one solid-state atomic ensemble. *Nature Communications*, 1:12, 2010.

[87] A Amari, A Walther, M Sabooni, M Huang, S Kröll, M Afzelius, I Usmani, B Lauritzen, N Sangouard, H de Riedmatten, and N Gisin. Towards an efficient atomic frequency comb quantum memory. *Journal of Luminescence*, 130(9):1579–1585, 2010.

[88] M Bonarota, J-L Le Gouët, and T Chanelière. Highly multimode storage in a crystal. *New Journal of Physics*, 13(1):13013, jan 2011.

[89] Nuala Timoney, Bjorn Lauritzen, Imam Usmani, Mikael Afzelius, and Nicolas Gisin. Atomic frequency comb memory with spin-wave storage in 153eu3+: Y2sio5. *Journal of Physics B: Atomic, Molecular and Optical Physics*, 45(12):124001, 2012.

[90] P Jobez, I Usmani, N Timoney, C Laplane, N Gisin, and M Afzelius. Cavity-enhanced storage in an optical spin-wave memory. *New Journal of Physics*, 16(8):83005, aug 2014.

[91] Mahmood Sabooni, Qian Li, Stefan Kröll, and Lars Rippe. Efficient quantum memory using a weakly absorbing sample. *Physical review letters*, 110(13):133604, 2013.

[92] M. D. Lukin, M. Fleischhauer, R. Cote, L. M. Duan, D. Jaksch, J. I. Cirac, and P. Zoller. Dipole blockade and quantum information processing in mesoscopic atomic ensembles. *Phys. Rev. Lett.*, 87:037901, Jun 2001.

[93] M Saffman and TG Walker. Creating single-atom and single-photon sources from entangled atomic ensembles. *Physical Review A*, 66(6):065403, 2002.

[94] Sylvain de Léséleuc, Daniel Barredo, Vincent Lienhard, Antoine Browaeys, and Thierry Lahaye. Analysis of imperfections in the coherent optical excitation of single atoms to rydberg states. *Phys. Rev. A*, 97:053803, May 2018.

[95] Jun Li, Ming-Ti Zhou, Chao-Wei Yang, Peng-Fei Sun, Jian-Long Liu, Xiao-Hui Bao, and Jian-Wei Pan. Semideterministic entanglement between a single photon and an atomic ensemble. *Phys. Rev. Lett.*, 123:140504, Oct 2019.

[96] Pascale Senellart, Glenn Solomon, and Andrew White. High-performance semiconductor quantum-dot single-photon sources. *Nature nanotechnology*, 12(11):1026, 2017.

[97] Xing Ding, Yu He, Z-C Duan, Niels Gregersen, M-C Chen, S Unsleber, Sebastian Maier, Christian Schneider, Martin Kamp, Sven Höfling, et al. On-demand single photons with high extraction efficiency and near-unity indistinguishability from a resonantly driven quantum dot in a micropillar. *Physical review letters*, 116(2):020401, 2016.

[98] Hui Wang, Hai Hu, T-H Chung, Jian Qin, Xiaoxia Yang, J-P Li, R-Z Liu, H-S Zhong, Y-M He, Xing Ding, et al. On-demand semiconductor source of entangled photons which simultaneously has high fidelity, efficiency, and indistinguishability. *Physical Review Letters*, 122(11):113602, 2019.

[99] YO Dudin and A Kuzmich. Strongly interacting rydberg excitations of a cold atomic gas. *Science*, 336(6083):887–889, 2012.

[100] YO Dudin, L Li, F Bariani, and A Kuzmich. Observation of coherent many-body rabi oscillations. *Nature Physics*, 8(11):790, 2012.

[101] Jun Li, Ming-Ti Zhou, Chao-Wei Yang, Peng-Fei Sun, Jian-Long Liu, Xiao-Hui Bao, and Jian-Wei Pan. Semideterministic entanglement between a single photon and an atomic ensemble. *Physical review letters*, 123(14):140504, 2019.

[102] Lucia Caspani, Chunle Xiong, Benjamin J Eggleton, Daniele Bajoni, Marco Liscidini, Matteo Galli, Roberto Morandotti, and David J Moss. Integrated sources of photon quantum states based on nonlinear optics. *Light: Science & Applications*, 6(11):e17100, 2017.

[103] Han-Sen Zhong, Yuan Li, Wei Li, Li-Chao Peng, Zu-En Su, Yi Hu, Yu-Ming He, Xing Ding, Weijun Zhang, Hao Li, Lu Zhang, Zhen Wang, Lixing You, Xi-Lin Wang, Xiao Jiang, Li Li, Yu-Ao Chen, Nai-Le Liu, Chao-Yang Lu, and Jian-Wei Pan. 12-photon entanglement and scalable scattershot boson sampling with optimal entangled-photon pairs from parametric down-conversion. *Phys. Rev. Lett.*, 121:250505, Dec 2018.

[104] Tian Zhong and Philippe Goldner. Emerging rare-earth doped material platforms for quantum nanophotonics. *Nanophotonics*, 2019.

[105] Morgan P Hedges, Jevon J Longdell, Yongmin Li, and Matthew J Sellars. Efficient quantum memory for light. *Nature*, 465(7301):1052, 2010.

[106] M Bonarota, J Ruggiero, J-L Le Gouët, and T Chanelière. Efficiency optimization for atomic frequency comb storage. *Physical Review A*, 81(3):033803, 2010.

[107] Zong-Quan Zhou, Wei-Bin Lin, Ming Yang, Chuan-Feng Li, and Guang-Can Guo. Realization of reliable solid-state quantum memory for photonic polarization qubit. *Physical review letters*, 108(19):190505, 2012.

[108] Mustafa Gündoğan, Patrick M Ledingham, Attaallah Almasi, Matteo Cristiani, and Hugues de Riedmatten. Quantum storage of a photonic polarization qubit in a solid. *Physical review letters*, 108(19):190504, 2012.

[109] Mikael Afzelius and Christoph Simon. Impedance-matched cavity quantum memory. *Physical Review A*, 82(2):022310, 2010.

[110] Mark Saffman, Thad G Walker, and Klaus Mølmer. Quantum information with rydberg atoms. *Reviews of Modern Physics*, 82(3):2313, 2010.

[111] Peter Lodahl, Sahand Mahmoodian, and Søren Stobbe. Interfacing single photons and single quantum dots with photonic nanostructures. *Reviews of Modern Physics*, 87(2):347, 2015.

[112] Hui Wang, Jian Qin, Xing Ding, Ming-Cheng Chen, Si Chen, Xiang You, Yu-Ming He, Xiao Jiang, L. You, Z. Wang, C. Schneider, Jelmer J. Renema, Sven Höfling, Chao-Yang Lu, and Jian-Wei Pan. Boson sampling with 20 input photons and a 60-mode interferometer in a 10^{14}-dimensional hilbert space. *Phys. Rev. Lett.*, 123:250503, Dec 2019.

[113] Inbal Friedler, Christophe Sauvan, Jean-Paul Hugonin, Philippe Lalanne, Julien Claudon, and Jean-Michel Gérard. Solid-state single photon sources: the nanowire antenna. *Optics express*, 17(4):2095–2110, 2009.

[114] Julien Claudon, Joël Bleuse, Nitin Singh Malik, Maela Bazin, Périne Jaffrennou, Niels Gregersen, Christophe Sauvan, Philippe Lalanne, and Jean-Michel Gérard. A highly efficient single-photon source based on a quantum dot in a photonic nanowire. *Nature Photonics*, 4(3):174, 2010.

[115] Marijn AM Versteegh, Michael E Reimer, Klaus D Jöns, Dan Dalacu, Philip J Poole, Angelo Gulinatti, Andrea Giudice, and Val Zwiller. Observation of strongly entangled photon pairs from a nanowire quantum dot. *Nature communications*, 5:5298, 2014.

[116] Tobias Huber, Ana Predojevic, Milad Khoshnegar, Dan Dalacu, Philip J Poole, Hamed Majedi, and Gregor Weihs. Polarization entangled photons from quantum dots embedded in nanowires. *Nano Letters*, 14(12):7107–7114, 2014.

[117] Klaus D Jöns, Lucas Schweickert, Marijn AM Versteegh, Dan Dalacu, Philip J Poole, Angelo Gulinatti, Andrea Giudice, Val Zwiller, and Michael E Reimer. Bright nanoscale source of deterministic entangled photon pairs violating bell's inequality. *Scientific reports*, 7(1):1700, 2017.

[118] Siddhartha Santra, Sreraman Muralidharan, Martin Lichtman, Liang Jiang, Chris R Monroe, and Vladimir S Malinovsky. Quantum repeaters based on two species trapped ions. *New Journal of Physics*, 2019.

[119] Nikolai Lauk, Neil Sinclair, Shabir Barzanjeh, Jacob P Covey, Mark Saffman, Maria Spiropulu, and Christoph Simon. Perspectives on quantum transduction. *Quantum Science and Technology*, 5(2):020501, 2020.